CMS Physics Analysis Summary

Contact: cms-pag-conveners-susy@cern.ch 2019/03/19

Search for physics beyond the standard model in events with two same-sign leptons or at least three leptons and jets in proton-proton collisions at $\sqrt{s} = 13$ TeV.

The CMS Collaboration

Abstract

A data sample of events from proton-proton collisions with two isolated same-sign leptons or at least three leptons, and at least two jets, is studied in a search for signatures of new physics phenomena by the CMS Collaboration at the LHC. The data correspond to an integrated luminosity of 137 fb^{-1}, at a center-of-mass energy of 13 TeV. The properties of the events are consistent with expectations from standard model processes, and no excess yield is observed. Exclusion limits at 95% confidence level are set on cross sections for the pair production of gluinos or squarks for various decay scenarios in the context of supersymmetry models conserving or violating R-parity. The observed lower mass limits are as high as 2.1 TeV for gluinos, and 0.9 TeV for top and bottom squarks.

1 Introduction

In the standard model (SM), the production in proton-proton (pp) collisions of multiple jets together with a same-sign (SS) dilepton pair, or three or more leptons, is only possible through very rare processes. These final states therefore provide an interesting starting point to search for physics beyond the Standard Model (BSM). In fact, many models of new physics trying to address the shortcomings of the SM can lead to such a signature in significant amount. Popular examples include the production of supersymmetric (SUSY) particles [1, 2], SS top quarks [3, 4], scalar gluons (sgluons) [5, 6], heavy scalar bosons of extended Higgs sectors [7, 8], and Majorana neutrinos [9], and vector-like quarks [10]. Both the ATLAS [11] and CMS [12, 13] Collaborations have recently carried out searches in these channels, using LHC data collected up to 2016.

In supersymmetric models [14–23], the decay chain of pair produced gluinos or squarks can contain multiple W or Z bosons, possibly including one or several pairs of SS W bosons. Such a decay chain is realized, for example, when a gluino decays into a top-antitop pair and a neutralino, or into a pair of quarks and a chargino that subsequently decays into a W boson and a neutralino. In R-parity conserving (RPC) scenarios, the lightest supersymmetric particle is neutral and stable and will therefore escape detection, leading to an imbalance of the measured transverse momentum, the magnitude of which can strongly depend on the model details, in particular on the mass spectrum of the various particles involved. R-parity violating (RPV) scenarios [24–26] additionally allow full decays of the SUSY particles into SM particles leading to signature with little or no missing transverse momentum ($p_{\mathrm{T}}^{\mathrm{miss}}$). For many SUSY models, the SS and multilepton signatures provide complementarity with searches in the zero or one lepton final states, and they are particularly relevant to probe compressed mass spectra and other scenarios involving low-momentum leptons or low $p_{\mathrm{T}}^{\mathrm{miss}}$.

In this note we extend the searches described in Ref. [12, 13], using a dataset of proton-proton collisions at $\sqrt{s} = 13\,\mathrm{TeV}$ recorded by the CMS detector at the LHC in 2016, 2017 and 2018 and corresponding to 137 fb^{-1}. Events with two SS or three or more light leptons (electrons and muons) and at least two hadronic jets are first selected and various signal regions (SRs) are then constructed based on variables such as the number of leptons, of jets (possibly identified as originating from b-quarks) or the $p_{\mathrm{T}}^{\mathrm{miss}}$ magnitude. A simultaneous comparison of the observed and SM expected yields in all signal regions is performed to set constraints on various BSM models detailed in Section 2. The main changes with respect to the previous analyses include the addition of low $p_{\mathrm{T}}^{\mathrm{miss}}$ signal regions, an optimization of the signal regions for the increased integrated luminosity, and the use of an improved b-jet identification algorithm.

2 Background and signal simulation

Monte Carlo (MC) simulations are used to study the various SM backgrounds as well as to estimate the event selection efficiency on the signals. Three sets of simulated events for each process are used in order to match the different data taking conditions in 2016, 2017 and 2018.

For most of the SM backgrounds, the hard scattering process is simulated with the MADGRAPH5_aMC@NLO 2.2.2 [27–29] or POWHEG v2 [30, 31] next-to-leading order (NLO) generators. New physics signal samples, as well as same-sign $\mathrm{W}^{\pm}\mathrm{W}^{\pm}$ and other very rare processes, are generated with MADGRAPH5_aMC@NLO at leading order (LO) precision, with up to two additional partons in the matrix element calculations. The set of parton distribution functions (PDF) used was updated from NNPDF3.0 [32] for the 2016 simulation to 3.1 [33] for 2017 and 2018 simulations.

Parton showering and hadronization, as well as the double-parton scattering production of $W^{\pm}W^{\pm}$, are described using the PYTHIA 8.2 generator [34] with the CUETP8M1 (2016 simulations) or CP5 (2017 and 2018) tunes [35–37]. The response of the CMS detector is modeled using the GEANT4 package [38] for background samples while the CMS fast simulation package [39] is used for signal samples.

To improve on the MADGRAPH modeling of the multiplicity of additional jets from initial-state radiation (ISR), MADGRAPH $t\bar{t}$ MC events are reweighted based on the number of ISR jets (N_J^{ISR}), so as to make the light flavor jet multiplicity in dilepton $t\bar{t}$ events agree with the one observed in data. The same reweighting procedure is applied to SUSY MC events corresponding to 2016 data. These reweighting factors vary between 1.46 and 0.77 for N_J^{ISR} between 1 and 4. We take one half of the deviation from unity as the systematic uncertainty in these reweighting factors. To account for possible mismodeling of the flavor of additional jets, an additional 70% uncertainty is applied to $t\bar{t}W$, $t\bar{t}Z$, and $t\bar{t}H$ events produced in association with a pair of b jets, reflecting the measured ratio of $t\bar{t}b\bar{b}$ / $t\bar{t}jj$ cross sections reported in Ref. [40].

The new physics signal models probed by this search are shown in Fig. 1 and 2. Production cross sections for these SUSY models are calculated at approximate-NNLO+NNLL order accuracy [41–47]. In each of the simplified SUSY models [48, 49] of Fig. 1, only two or three new particles have masses sufficiently low to be produced on-shell, the branching fraction for the decays shown are assumed to be 100%, and the decays are assumed to be prompt. Gluino pair production models giving rise to signatures with up to four b quarks and up to four W bosons are shown in Figs. 1a–c. In these models, the gluino decays to the lightest squark ($\tilde{g} \to \tilde{q}q$), which in turn decays to same-flavor ($\tilde{q} \to q\tilde{\chi}_1^0$) or different-flavor ($\tilde{q} \to q'\tilde{\chi}_1^{\pm}$) quarks. The chargino decays to a W boson and a neutralino ($\tilde{\chi}_1^{\pm} \to W^{\pm}\tilde{\chi}_1^0$), where the $\tilde{\chi}_1^0$ escapes detection and is taken to be the lightest SUSY particle (LSP).

The first scenario, considered in Fig. 1a, includes an off-shell third-generation squark ($\tilde{t}$) leading to the three-body decay of the gluino, $\tilde{g} \to t\bar{t}\tilde{\chi}_1^0$ (T1tttt) resulting in events with four W bosons and four b quarks. The model shown in Fig. 1b (T5tttt) includes an on-shell top squark with mass splitting between the $\tilde{t}$ and the $\tilde{\chi}_1^0$ equal to the top quark mass ($m_{\tilde{t}} - m_{\tilde{\chi}_1^0} = m_t$), with a $\tilde{t} \to t\tilde{\chi}_1^0$ decay. In Fig. 1c, the decay process includes a virtual light flavor squark, leading to three-body decays of $\tilde{g} \to qq'\tilde{\chi}_1^{\pm}$ or $\tilde{g} \to qq'\tilde{\chi}_2^0$, with a resulting signature of two W bosons, two Z bosons, or one of each, and four light flavor jets. This model, T5qqqqWZ, is studied with two different assumptions for the chargino mass: $m_{\tilde{\chi}_1^{\pm}} = 0.5(m_{\tilde{g}} + m_{\tilde{\chi}_1^0})$, and $m_{\tilde{\chi}_1^{\pm}} = m_{\tilde{\chi}_1^0} + 20\,\text{GeV}$, producing on- and off-shell bosons, respectively. The model is also considered with the assumption of decays to two W bosons exclusively (T5qqqqWW).

Fig. 1d shows a model of bottom squark production with a subsequent decay of $\tilde{b} \to t\tilde{\chi}_1^{\pm}$, yielding two b quarks and four W bosons. This model, T6ttWW, is considered as a function of the $\tilde{b}$ and $\tilde{\chi}_1^{\pm}$ masses. The $\tilde{\chi}_1^0$ mass is fixed to be 50 GeV, causing two of the W bosons to be produced off-shell when the $\tilde{\chi}_1^0$ mass is close to that of the $\tilde{\chi}_1^{\pm}$. Finally, Fig. 1e displays a model similar to T6ttWW, but with top squark pair production and a subsequent $\tilde{t}_2 \to \tilde{t}_1 H/Z$ decay, producing final states with two H bosons, two Z bosons, or one of each. In this T6ttHZ model, the $\tilde{\chi}_1^0$ mass is taken such that $m(\tilde{t}_2) - m(\tilde{\chi}_1^0) = 175\,\text{GeV}$.

All the above models assume conservation of R-parity. We also consider two additional cases where R-parity is not conserved. In T1qqqqL (Fig 2, left), the gluino decays to the lightest squark ($\tilde{g} \to \tilde{q}q$) which in turn decays to a quark ($\tilde{q} \to q\tilde{\chi}_1^0$), but the $\tilde{\chi}_1^0$ is off-shell and decays (violating R-parity) into two quarks and a charged lepton, giving rise to a prompt 5-body decay of the gluino. In T1tbs (Fig 2, right) each gluino decays into three different SM quarks (a top, a

bottom, and a strange quark).

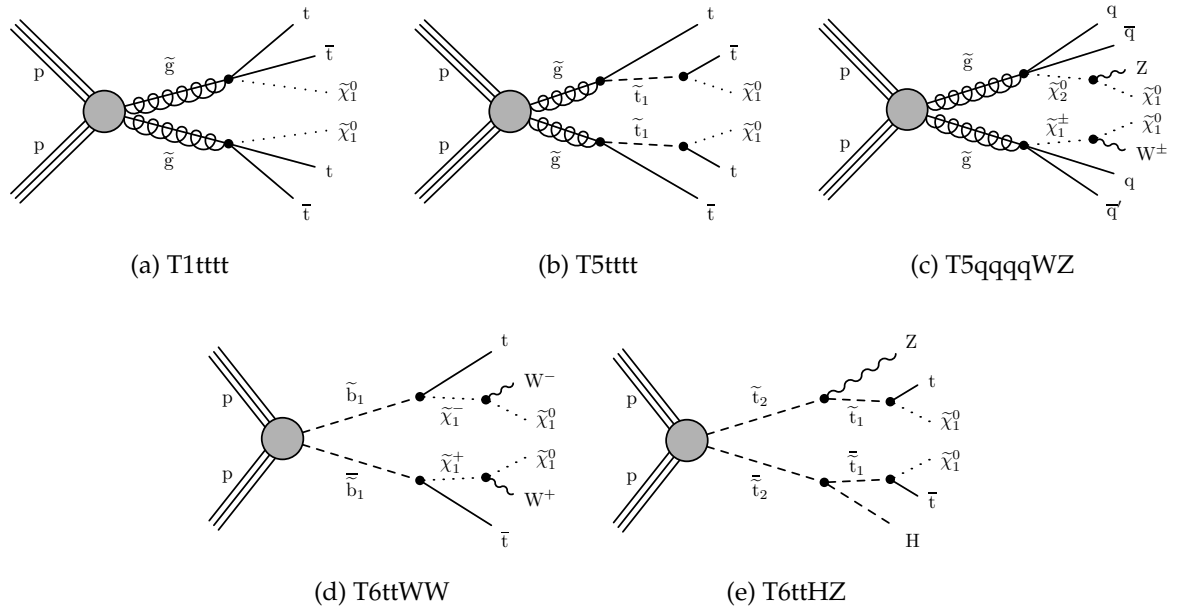

(a) T1tttt (b) T5tttt (c) T5qqqqWZ

(d) T6ttWW (e) T6ttHZ

Figure 1: Diagrams illustrating the simplified RPC SUSY models considered in this analysis.

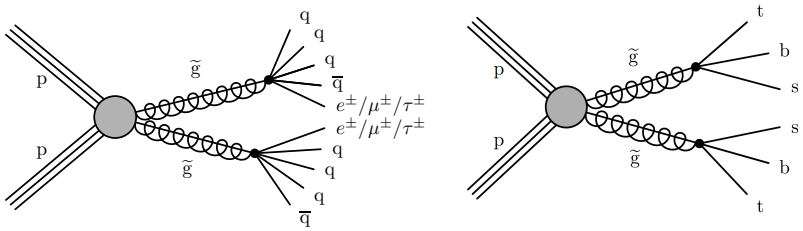

Figure 2: Diagrams illustrating the two RPV SUSY models considered in this analysis.

3 The CMS detector and event reconstruction

The central feature of the CMS detector is a superconducting solenoid of 6 m internal diameter, providing a magnetic field of 3.8 T. Within the solenoid volume are a silicon pixel and strip tracker, a lead tungstate crystal electromagnetic calorimeter (ECAL), and a brass and scintillator hadron calorimeter (HCAL), each composed of a barrel and two endcap sections. Forward calorimeters extend the pseudorapidity (η) coverage provided by the barrel and endcap detectors. Muons are detected in gas-ionization chambers embedded in the steel flux-return yoke outside the solenoid. A more detailed description of the CMS detector, together with a definition of the coordinate system used and the relevant kinematic variables, can be found in Ref. [50].

Events of interest are selected using a two-tiered trigger system [51]. The first level (L1), composed of custom hardware processors, uses information from the calorimeters and muon detectors to select events at a rate of around 100 kHz within a time interval of less than 4 μs. The second level, known as the high-level trigger, consists of a farm of processors running a version of the full event reconstruction software optimized for fast processing, and reduces the event rate to around 1 kHz before data storage.

The particle-flow algorithm [52] aims to reconstruct and identify each individual particle in an event, with an optimized combination of information from the various elements of the CMS detector. The energy of photons is directly obtained from the ECAL measurement. The energy of electrons is determined from a combination of the electron momentum at the primary interaction vertex as determined by the tracker, the energy of the corresponding ECAL cluster, and the energy sum of all bremsstrahlung photons spatially compatible with the electron track [53]. The momentum of muons is obtained from the curvature of the corresponding track, combining information from the silicon tracker and the muon system [54]. The energy of charged hadrons is determined from a combination of their momentum measured in the tracker and the matching ECAL and HCAL energy deposits, corrected for the response function of the calorimeters to hadronic showers. The energy of neutral hadrons is obtained from the corresponding corrected ECAL and HCAL energies.

Hadronic jets are clustered from neutral PF candidates and charged PF candidates associated with the primary vertex, using the anti-k_{T} algorithm [55, 56] with a distance parameter of 0.4. The jet momentum is determined as the vectorial sum of all PF candidate momenta in the jet. An offset correction is applied to jet energies to take into account the contribution from pileup. Jet energy corrections are derived from simulation, and are improved with in situ measurements of the energy balance in dijet, multijet, γ +jet and leptonically decaying Z+jet events [57, 58]. Additional selection criteria are applied to each jet to remove jets potentially dominated by instrumental effects or reconstruction failures. Jets originating from b quarks are identified as b-tagged jets using a deep neural network algorithm [59], with a working point chosen such that the efficiency to identify a b jet is 55–70% for a jet transverse momentum (p_{T}) between 20 and 400 GeV. The misidentification rate for a light-flavor jet is 1–2% in the same jet p_{T} range. The vector $\vec{p}_{\mathrm{T}}^{\,\mathrm{miss}}$ is defined as the projection on the plane perpendicular to the beams of the negative vector sum of the momenta of all reconstructed PF candidates in an event [60]. Its magnitude, called missing transverse momentum, is referred to as $p_{\mathrm{T}}^{\mathrm{miss}}$. The scalar p_{T} sum of all jets in an event is referred to as H_{T}.

4 Event selection and search strategy

The search strategy is similar to the one adopted in Ref. [12, 13]. A generic event selection is applied requiring the presence of at least two hadronic jets and at least two leptons, including a SS pair. Each selected event is then assigned to a SR, based on its content. Such a strategy ensures sensitivity to a broad range of possible signatures of new physics, even beyond the signal benchmarks considered. The normalization of the various backgrounds is constrained by taking advantage of the change of the background composition between SRs, and relying on differences between signal and background kinematics.

The basic kinematic requirements applied to leptons and jets are presented in Table 1. The analysis requires a minimum of two jets with p_{T} >40 GeV and two light leptons with $p_T >$ 10/15 GeV depending on their flavor (muon/electron). Specific isolation and identification conditions, similar to those described in Ref. [61], are applied on leptons. They aim in particular at recovering leptons overlapping with a jet due to the high hadronic activity present in most of the considered signal models.

In order to reject low mass dilepton pairs arising from the decay of c- and b-hadrons or from the Drell-Yan process, a loose lepton selection is used to identify additional leptons, and events where a loose lepton forms an opposite-sign (OS) same flavor pair with an invariant mass ($m_{\ell\ell}$) less than 12 GeV are rejected. Furthermore events containing a dilepton pair with $m_{\ell\ell} < 8\,\mathrm{GeV}$ regardless of charge or flavor are rejected in order to emulate a similar condition applied at

Table 1: p_T and η requirements for leptons and jets. Note that the p_T thresholds to count jets and b-tagged jets are different.

Object	p_T (GeV)	$\lvert\eta\rvert$
Electrons	> 15	< 2.5
Muons	> 10	< 2.4
Jets	> 40	< 2.4
b-tagged jets	> 25	< 2.4

trigger level. When several SS pairs are found, muons take precedence over electrons, and amongst same flavor pairs, the one with the highest lepton p_T sum is selected. Events are then labelled according to the p_T of the leptons forming the SS pair: high-high (HH) if both have $p_T > 25\,\text{GeV}$, low-low (LL) if both have $p_T < 25\,\text{GeV}$ and high-low (HL) otherwise.

Two sets of trigger algorithms are used to select the events: pure dilepton triggers which require the presence of two isolated leptons with p_T thresholds on the first (second) lepton in the 17-23 GeV (8-12 GeV) range, and non isolated dilepton triggers with a p_T threshold at 8 GeV on both leptons and with an additional condition on the presence of hadronic activity: $H_T > 300 - 350\,\text{GeV}$. The former is used to select HH and HL pairs while LL pairs are selected using the latter.

Six exclusive categories are then built:

- SSHH: exactly 2 leptons, both with $p_T > 25\,\text{GeV}$, and $p_T^{\text{miss}} > 50\,\text{GeV}$.
- SSHL: exactly 2 leptons, one with $p_T > 25\,\text{GeV}$, one with $p_T < 25\,\text{GeV}$ and $p_T^{\text{miss}} > 50\,\text{GeV}$.
- SSLL: exactly 2 leptons, both with $p_T < 25\,\text{GeV}$ and $p_T^{\text{miss}} > 50\,\text{GeV}$.
- LM (low p_T^{miss}): exactly 2 leptons, both with $p_T > 25\,\text{GeV}$, and $p_T^{\text{miss}} < 50\,\text{GeV}$.
- ML (multilepton): ≥ 3 leptons, at least one with $p_T > 25\,\text{GeV}$, $p_T^{\text{miss}} > 50\,\text{GeV}$.

Various SRs are constructed, based on the following variables: the jet multiplicity N_{jets}, the b-tagged jet multiplicity N_b, H_T, p_T^{miss}. For ML regions, the presence of a Z candidate formed by a pair of OS same flavor leptons with $76 < m_{\ell\ell} < 106\,\text{GeV}$ is used to separate on-Z and and off-Z SRs. An additional variable introduced in Ref. [61], m_T^{min}, is also used in all categories except LM. This variable is characterized by a kinematic cutoff for events where p_T^{miss} only arises from the leptonic decay of a single W boson and is therefore very effective at discriminating signal and background signatures. It is defined as the minimum transverse mass calculated between each of the leptons forming the SS pair and $\vec{E}_T^{\text{miss}}$, except for the on-Z ML regions where the transverse mass is only computed using the leptons not forming the Z candidate. Finally, in order take advantage of the charge asymmetry in most of the background processes such as WZ, $t\bar{t}W$ or SS WW, some SRs are also divided according to the charge sum of the lepton pair. The SRs corresponding to each category, SSHH, SSHL, SSLL, LM and ML, are summarized in Tables 2, 3, 4, 5, and 6, respectively. The binning ranges are chosen in order to maximize the sensitivity to a few SUSY benchmark points and such that the expected yields in each SRs are never much lower than one event.

The lepton reconstruction and identification efficiency is in the range of 45–70% (70–90%) for electrons (muons) with $p_T > 25\,\text{GeV}$, increasing as a function of p_T and converging to the maximum value for $p_T > 60\,\text{GeV}$. In the low-momentum regime, $15 < p_T < 25\,\text{GeV}$ for electrons and $10 < p_T < 25\,\text{GeV}$ for muons, the efficiencies are 40% for electrons and 55% for muons. The lepton trigger efficiency for electrons is in the range of 90-98%, converging to the

maximum value for $p_T > 30\,\text{GeV}$, and around 92% for muons. The efficiencies of the H_T and p_T^{miss} requirements are mostly determined by the jet energy and p_T^{miss} resolutions, which are discussed in Refs. [57, 62, 63].

Table 2: SR definitions for the SSHH category. Charge split cells are indicated with (++) and (--). In order to avoid overlaps, an upper bound $p_T^{\text{miss}} < 300\,\text{GeV}$ is used for regions with $H_T > 300\,\text{GeV}$. There are 62 regions in total.

N_b	m_T^{min} (GeV)	p_T^{miss} (GeV)	N_{jets}	$H_T < 300\,\text{GeV}$	$H_T \in [300, 1125]$ GeV	$H_T \in [1125, 1300]$ GeV	$H_T \in [1300, 1600]$ GeV	$H_T > 1600\,\text{GeV}$
0	< 120	$50 - 200$	2-4	SR1	SR2	SR54 $N_{\text{jets}} < 5$	SR55 $N_{\text{jets}} < 5$	SR56 $N_{\text{jets}} < 5$
			5+	SR3	SR4			
		$200 - 300$	2-4		SR5 (++) / SR6 (--)			
			5+		SR7			
	> 120	$50 - 200$	2-4		SR8 (++) / SR9 (--)			
			5+		SR10			
		$200 - 300$	2-4					
			5+					
1	< 120	$50 - 200$	2-4	SR11	SR12	SR57 $N_{\text{jets}} = 5$ or 6	SR58 $N_{\text{jets}} = 5$ or 6	SR59 $N_{\text{jets}} = 5$ or 6
			5+	SR13 (++) / SR14 (--)	SR15 (++) / SR16 (--)			
		$200 - 300$	2-4		SR17 (++) / SR18 (--)			
			5+		SR19			
	> 120	$50 - 200$	2-4		SR20 (++) / SR21 (--)			
			5+		SR22			
		$200 - 300$	2-4					
			5+					
2	< 120	$50 - 200$	2-4	SR23	SR24	SR60 $N_{\text{jets}} > 6$	SR61 $N_{\text{jets}} > 6$	SR62 $N_{\text{jets}} > 6$
			5+	SR25 (++) / SR26 (--)	SR27 (++) / SR28 (--)			
		$200 - 300$	2-4		SR29 (++) / SR30 (--)			
			5+		SR31			
	> 120	$50 - 200$	2-4		SR32 (++) / SR33 (--)			
			5+		SR34			
		$200 - 300$	2-4					
			5+					
3+	< 120	$50 - 200$	2-4	SR35 (++) / SR36 (--)	SR37 (++) / SR38 (--)			
			5+		SR39 (++) / SR40 (--)			
		$200 - 300$	2-4		SR37 (++) / SR38 (--)			
			5+		SR39 (++) / SR40 (--)			
	> 120	> 50	2-4	SR41	SR42 (++) / SR43 (--)			
			5+		SR44 (++) / SR45 (--)			
inclusive	inclusive	$300 - 500$	2-4		SR46 (++) / SR47 (--)			
		> 500			SR48 (++) / SR49 (--)			
		$300 - 500$	5+		SR50 (++) / SR51 (--)			
		> 500			SR52 (++) / SR53 (--)			

Table 3: SR definitions for the SSHL category. In order to avoid overlaps, an upper bound $p_T^{\text{miss}} < 300\,\text{GeV}$ is used for regions with $H_T > 300\,\text{GeV}$. There are 43 regions in total.

N_b	m_T^{min} (GeV)	p_T^{miss} (GeV)	N_{jets}	$H_T < 300\,\text{GeV}$	$H_T \in [300, 1125]$ GeV	$H_T \in [1125, 1300]$ GeV	$H_T > 1300\,\text{GeV}$
0	< 120	$50 - 200$	2-4	SR1	SR2	SR40 (++) / SR41 (--)	SR42 (++) / SR43 (--)
			5+	SR3	SR4		
		$200 - 300$	2-4		SR5 (++) / SR6 (--)		
			5+		SR7		
1	< 120	$50 - 200$	2-4	SR8	SR9		
			5+	SR10 (++) / SR11 (--)	SR12 (++) / SR13 (--)		
		$200 - 300$	2-4		SR14		
			5+		SR15 (++) / SR16 (--)		
2	< 120	$50 - 200$	2-4	SR17	SR18		
			5+	SR19 (++) / SR20 (--)	SR21 (++) / SR22 (--)		
		$200 - 300$	2-4		SR23 (++) / SR24 (--)		
			5+		SR25		
3+	< 120	$50 - 200$	2+	SR26 (++) / SR27 (--)	SR28 (++) / SR29 (--)		
		$200 - 300$			SR30		
inclusive	> 120	$50 - 300$	2+	SR31	SR32		
inclusive	inclusive	$300 - 500$	2-4		SR33 (++) / SR34 (--)		
		> 500			SR35 (++) / SR36 (--)		
		$300 - 500$	5+		SR37 (++) / SR38 (--)		
		> 500			SR39		

Table 4: SR definitions for the SSLL category. All SRs in this category require $N_{\text{jets}} \geq 2$. There are 8 regions in total.

N_{b}	$m_{\text{T}}^{\text{min}}$ (GeV)	H_{T} (GeV)	$p_{\text{T}}^{\text{miss}} \in [50, 200]$ GeV	$p_{\text{T}}^{\text{miss}} > 200$ GeV
0	< 120	> 400	SR1	SR2
1			SR3	SR4
2			SR5	SR6
≥ 3			SR7	
Inclusive	> 120		SR8	

Table 5: SR definitions for the LM category. All SRs in this category require $N_{\text{jets}} \geq 2$, $p_{\text{T}}^{\text{miss}} < 50$ GeV, $H_{\text{T}} > 300$ GeV, and HH lepton momenta. The 2 high H_{T} regions are split only by N_{jets}, giving 11 regions in total.

N_{b}	N_{jets}	$H_{\text{T}} \in [300, 1125]$ GeV	$H_{\text{T}} \in [1125, 1300]$ GeV	$H_{\text{T}} > 1300$ GeV
0	2-4	SR1	SR8 ($N_{\text{jets}} < 5$)	SR10 ($N_{\text{jets}} < 5$)
	5+	SR2		
1	2-4	SR3		
	5+	SR4		
2	2-4	SR5	SR9 ($N_{\text{jets}} \geq 5$)	SR11 ($N_{\text{jets}} \geq 5$)
	5+	SR6		
≥ 3	2+	SR7		

Table 6: SR definitions for the ML category. All SRs in these categories require $N_{\text{jets}} \geq 2$. Regions marked with † are split by $m_{\text{T}}^{\text{min}} = 120$ GeV, with the high $m_{\text{T}}^{\text{min}}$ region specified by the second label. On-Z regions events include an OS same flavor lepton pair with $76 < m_{\ell\ell} < 106$ GeV. There are 44 regions in total.

		off-Z			on-Z		
N_{b}	H_{T} (GeV)	$p_{\text{T}}^{\text{miss}} \in [50, 150]$ GeV	$p_{\text{T}}^{\text{miss}} \in [150, 300]$ GeV	$p_{\text{T}}^{\text{miss}} \geq 300$ GeV	$p_{\text{T}}^{\text{miss}} \in [50, 150]$ GeV	$p_{\text{T}}^{\text{miss}} \in [150, 300]$ GeV	$p_{\text{T}}^{\text{miss}} \geq 300$ GeV
0	<400	SR1/SR2†	SR3/SR4†	SR20/SR21†	SR22/SR23†	SR24/SR25†	SR43/SR44†
	400-600	SR5	SR6		SR26/SR27†	SR28/SR29†	
1	<400	SR7	SR8		SR30	SR31	
	400-600	SR9	SR10		SR32	SR33	
2	<400	SR11	SR12		SR34	SR35	
	400-600	SR13	SR14		SR36	SR37	
≥ 3	<600	SR15			SR38		
Inclusive	≥ 600	SR16/SR17†	SR18/SR19†		SR39/SR40†	SR41/SR42†	

5 Backgrounds

Several standard model processes can lead to the signatures studied in this analysis. There are three background categories, depending on the lepton content of the event:

- Events with two or more prompt leptons, including a SS pair.
- Events with at least one nonprompt or fake lepton.
- Events with a pair of opposite sign leptons, one of them mistakenly reconstructed with the wrong charge.

The first category includes a variety of low cross section processes where multiple electroweak bosons are produced (possibly in the decay of a top quark) and decay leptonically, leading to a SS lepton pair. This category usually dominates the background yields in SRs with large $p_{\mathrm{T}}^{\mathrm{miss}}$ or H_{T} and in most of the ML SRs with a Z candidate. The dominant processes are the production of a WZ or a same sign W pair, or of a $\mathrm{t\bar{t}}$ pair in association with a W, Z or Higgs boson. Each of them is treated separately in this analysis. More rare processes (including ZZ, triple boson production, tWZ, tZq, $\mathrm{t\bar{t}t\bar{t}}$ and double parton scattering) are also considered. Their expected yields are summed up into a single contribution called "Rares". Finally various processes including a real photon such as $\mathrm{W}\gamma$, $\mathrm{Z}\gamma$, $\mathrm{t\bar{t}}\gamma$, and $\mathrm{t}\gamma$, are also considered. They are also grouped together and referred to as "X+γ". All these contributions are estimated using simulated samples, with correction factors applied to take into account the small differences between data and the simulation as also discussed in Section 6.

The second category consists of events when one of the selected leptons, generically denoted "nonprompt lepton", is either a misidentified hadron or a decay product of a heavy- or light-flavor hadron. This category is typically the dominant one in signal regions with moderate or low $p_{\mathrm{T}}^{\mathrm{miss}}$ or low $m_{\mathrm{T}}^{\mathrm{min}}$ (except in the on-Z ML SRs). This background is estimated directly from the data, using the "tight-to-loose" method, as already used in the previous version of this analysis [12, 13]. The method is based on measuring the probability for a nonprompt lepton passing loose selection criteria to also pass the tight selection used in the analysis (tight-to-loose ratio). The number of events with a given number N of tight leptons, including at least one nonprompt lepton, can then be inferred applying the measured probability to events with N loose leptons, but with at least one of the leptons failing the tight selection. The measurement is performed using a sample enriched in dijet events and containing exactly one loose lepton, low $p_{\mathrm{T}}^{\mathrm{miss}}$ and low $m_{\mathrm{T}}^{\mathrm{min}}$. The prompt lepton contamination in this sample is estimated using the $m_{\mathrm{T}}^{\mathrm{min}}$ distribution in data, and it is subtracted before calculating the tight-to-loose ratio. The tight-to-loose ratio is computed separately for electrons and muons, and it is parametrized as a function of the lepton η and $p_{\mathrm{T}}^{\mathrm{corr}}$. The $p_{\mathrm{T}}^{\mathrm{corr}}$ variable is defined as the sum of the lepton p_{T} and the transverse momentum of other PF candidates found in the isolation cone that exceeds the isolation threshold value applied to tight leptons. This variable is found to be more correlated to the parent parton p_{T} than the lepton p_{T} itself and therefore improves the fake rate stability across kinematic variables such as H_{T}. The performance of the tight-to-loose method was tested in simulated $t\bar{t}$ and W+jets simulated samples by comparing the number of SS lepton pairs predicted by the method to the actual observed number of such pairs. The two estimates were compared as a function of kinematic properties and found to agree within 30%.

The final category is a subdominant background in all SRs and corresponds to events where the charge of a prompt lepton is mismeasured. Charge misidentification is a rare situation that can occur when an electron undergoes a strong bremsstrahlung in the tracker. Similarly to the tight-to-loose method, the number of SS lepton pairs where one of the lepton has its charge flipped can be determined using the number of opposite-sign pairs and the knowledge of the

charge misidentification rate. We use simulations to parametrize this rate as a function of p_{T} and η for electrons and find values varying between 10^{-5} (central electrons with $p_{\mathrm{T}} \approx 20$ GeV) and 0.5% (forward electrons with $p_{\mathrm{T}} \approx 200$ GeV). The same sign dielectron mass distribution in the Z peak region in data and simulations is used to derive a correction factor. Good agreement is found in 2016 while the simulations corresponding to 2017 and 2018 data are scaled by 1.4. No significant p_T dependency is observed in this scale factor. Muon charge mismeasurement is found to be at least one order of magnitude smaller than electrons in simulation and is therefore neglected.

6 Systematic uncertainties

The predicted yields of signal and background processes are affected by several sources of uncertainty, summarized in Table 7. Depending on their source, they are treated as fully correlated or uncorrelated between the three years of data taking. Signals and backgrounds estimated from simulation are affected by experimental uncertainties on the efficiency of the trigger and lepton reconstruction and identification [53, 54], the efficiency of b tagging [59], the jet energy scale [57], the integrated luminosity [64], and the value of the inelastic cross section, which affects the pileup rate [65]. Simulation is also affected by theoretical uncertainties, which are evaluated by varying the factorization and renormalization scales by a factor of two, and by using replicas of the NNPDF3.0 and 3.1 sets [32, 33, 66]. These uncertainties can affect both the overall yield (normalization) and the relative population (shape) across SRs. Background normalization uncertainties are increased to 30%, either to account for the additional hadronic activity required (for WZ and $\mathrm{W^{\pm}W^{\pm}}$) or to take into consideration recent measurements (for $\mathrm{t\bar{t}W}$, $\mathrm{t\bar{t}Z}$) [67, 68]. The Rare and X+γ backgrounds, which are less well known, are assigned a 50% uncertainty.

For the backgrounds estimated using data, nonprompt lepton and charge misidentification, the normalization and shape uncertainties have dedicated estimates. Statistical uncertainties on data yields in control regions affect both methods, and are taken into account. In addition, the nonprompt lepton background is assigned a 30% uncertainty derived from closure tests as a function of event kinematic properties in simulation, and the uncertainty on prompt lepton contamination is propagated resulting in a 1–30% additional uncertainty on the background yields. The charge misidentification background is assigned a 20% uncertainty based on the agreement as a function of event kinematic properties between the estimate and data in $\mathrm{Z} \to \mathrm{e^{+}e^{-}}$ events with one electron or positron having a misidentified charge.

7 Results and interpretation

Figure 3 presents, for the full set of events selected in this analysis, the expected and observed distributions of the variables used to define the various SRs. Overall data yields exceed expectation by an amount close to the systematic uncertainty. No particular trend is however seen in the distributions.

The full results of the search in each SR are presented in Figures 4 and 5 and summarized in Table 8, while yield tables with breakdowns for each background are included in Appendix A. No significant deviation with respect to the SM background prediction is observed. The largest excess after performing a background-only fit to the data is found in SR HH54. It corresponds to 2.6 standard deviation (σ). The only other SR with more than a 2σ excesses is LM7 (2.3σ). For the case of HH54, the neighboring bin HH55, which is adjacent along the H_{T} dimension, has a significance of -1.6σ.

Table 7: Summary of the sources of uncertainty and their effect on the yields of different processes in the SRs. The first two groups list experimental and theoretical uncertainties assigned to processes estimated using simulation, while the last group lists uncertainties assigned to processes whose yield is estimated from data. The uncertainties in the first group also apply to signal samples. Reported values are representative for the most relevant signal regions.

Source	Typical uncertainty (%)	Correlation across years
Integrated luminosity	2.3-2.5	Uncorrelated
Lepton selection	$2-10$	Uncorrelated
Trigger efficiency	$2-7$	Uncorrelated
Pileup	$0-6$	Uncorrelated
Jet energy scale	$1-15$	Uncorrelated
b tagging	$1-10$	Uncorrelated
Simulated sample size	$1-20$	Uncorrelated
Scale and PDF variations	$10-20$	Correlated
Theoretical background cross sections	$30-50$	Correlated
Nonprompt leptons	30	Correlated
Charge misidentification	20	Uncorrelated

These results are then interpreted as experimental constraints on the signal models discussed in Section 2. For each signal model, results from all SRs are used to obtain an exclusion limit at the 95% confidence level (CL) with an asymptotic formulation of the modified frequentist CL_s criterion [69–72]. Compared to the previous versions of the analysis [12, 13], the results extend the gluino and squark mass expected exclusion by up to 200 GeV due to the increase in the integrated luminosity and the optimization of SR definitions. Two additional models are included to demonstrate the sensitivity of the analysis to RPV scenarios.

Figure 6 shows observed and expected cross section limits for simplified models of gluino pair production with each gluino decaying off- or on-shell to third-generation squarks. These models were introduced in Section 2 and denoted as T1tttt and T5tttt. Similarly, Figure 7 and 8 show the corresponding limits for gluino pair production models followed by a decay through off-shell first- or second-generation squarks and a chargino. Two different assumptions are made on the chargino mass, taken to be between that of the gluino and the LSP. The T5qqqqWW model results in no b quarks and either on-shell or off-shell W bosons. The T5qqqqWZ model assumes an equiprobable decay of the gluino into $\widetilde{\chi}_1^+$, $\widetilde{\chi}_1^-$, or $\widetilde{\chi}_2^0$. In addition, Fig. 9 shows the exclusion limits of the T6ttWW model with bottom squark pair production followed by a decay through a chargino, resulting in two b quarks and four W bosons. Figure 10 shows exclusion limits of the T6ttHZ model with second-generation top squark pair production decaying into first-generation top squark and a Z or H boson. The three sets of exclusion limits correspond to $B(\widetilde{t}_2 \to \widetilde{t}_1 Z)$ of 0, 50, and 100%. Compared to previous publications, for all of the RPC models probed, the reach of the previous analysis is extended by 150–200 GeV and observed (expected) exclusion limits are 1.6 (1.8), 1.1 (1.1) and 0.9 (1.0) TeV for gluino, LSP, and bottom squark masses, respectively.

Furthermore, Figure 11 shows observed and expected limits of SUSY cross sections as a function of gluino masses with two RPV models described in Section 2. The T1qqqqL model assumes gluino pair production followed by a five-body flavor-democratic decay to four light quarks and one leptons via RPV. The T1tbs model assumes also gluino pair production followed by a three-body decay to a top, bottom and strange quark. Observed (expected) exclusion limits are set on the gluino mass of 2.1 (2.1) TeV for T1qqqqL and 1.7 (1.7) TeV for T1tbs respectively.

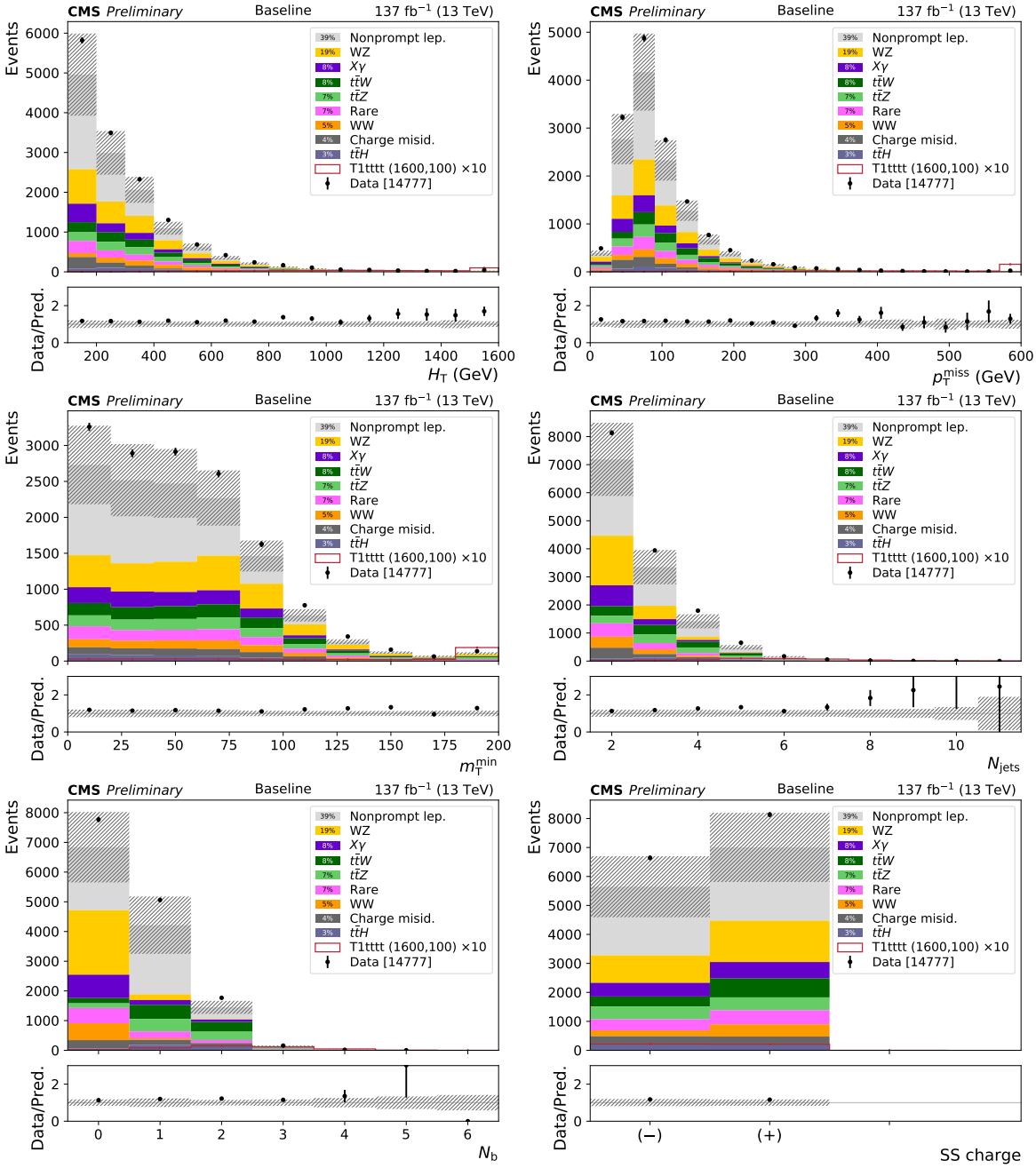

Figure 3: Distributions of the main analysis variables after the baseline selection in all signal categories: H_T, p_T^{miss}, m_T^{min}, N_{jets}, N_b, and the charge of the same sign pair, where the last bin includes the overflow. The hatched area represents the total uncertainty in the background prediction. The lower panels show the ratio of the observed event yield and the background prediction.

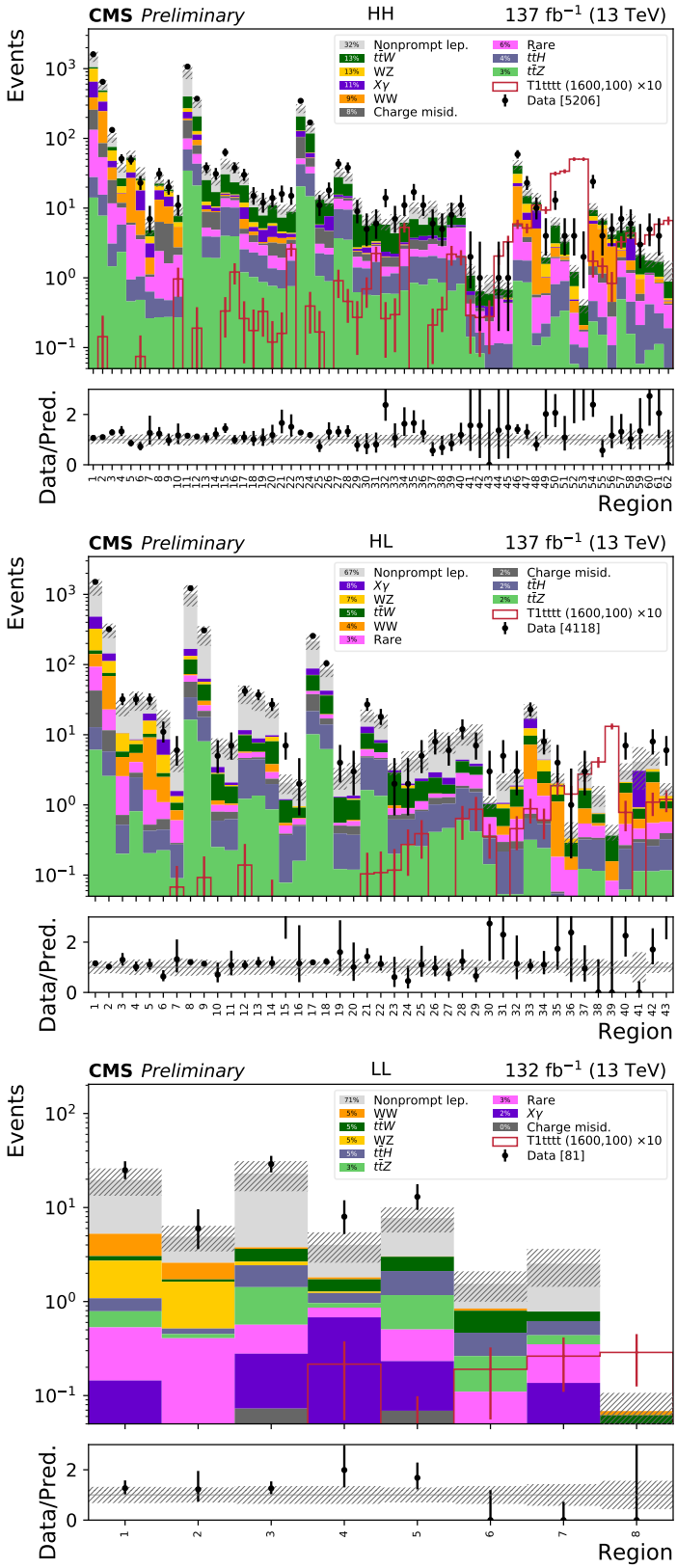

Figure 4: Expected and observed SR yields for the SSHH, SSHL, SSLL signal categories.

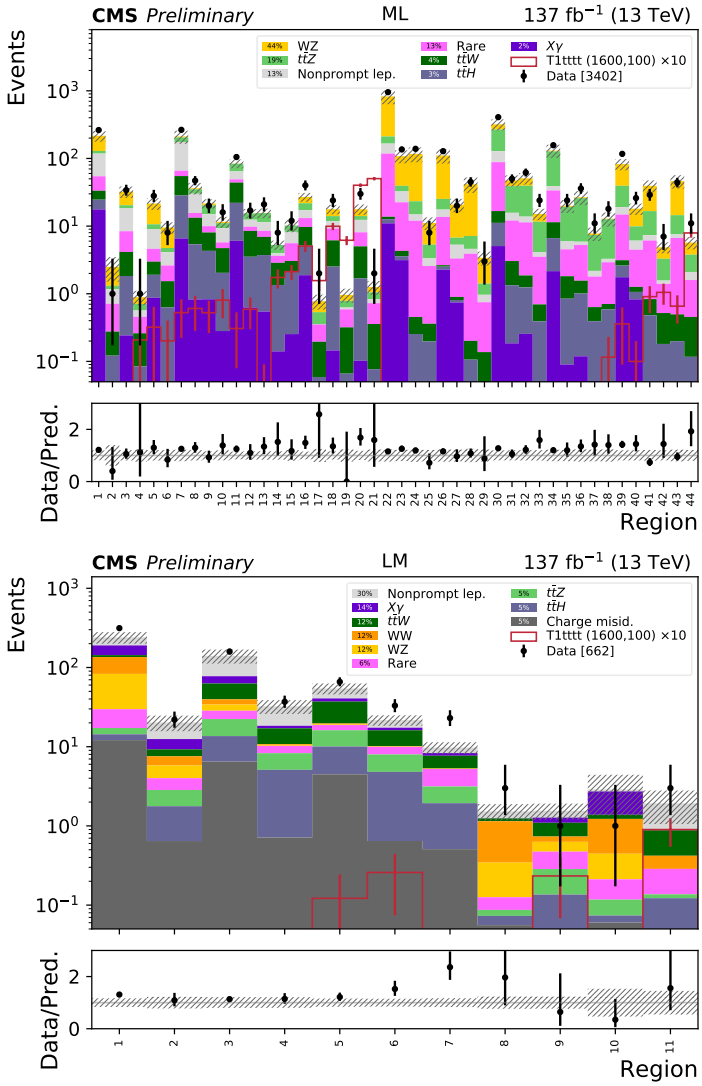

Figure 5: Expected and observed SR yields for the ML and LM signal categories.

Table 8: Expected background and observed event yields in the search regions used in this search.

	HH regions		HL regions		LL regions		ML regions		LM regions	
	Expected SM	Observed	Expected SM	Observed	Expected SM	Observed	Expected SM	Observed	Expected SM	Observed
SR1	1510±310	1609	1300±310	1504	20±6	25	220±40	263	240±50	314
SR2	590±90	647	310±70	319	4.9±1.5	6	2.5±2.5	1	20±5	22
SR3	103±22	132	25±6	32	23±6	29	32±6	34	140±31	159
SR4	38±7	51	32±8	32	4±4	8	0.9±0.5	1	32±7	37
SR5	57±10	49	29±6	32	7.7±2.1	13	22±4	28	54±8	66
SR6	32±9	23	17±6	11	1.5±0.8	0	9.5±1.8	8	22±4	33
SR7	5.5±1.7	7	4.5±2.5	6	2.5±1.2	0	210±40	265	9.7±2.1	23
SR8	25±6	31	1010±250	1223	0.07±0.07	0	36±6	47	1.5±0.5	3
SR9	21±5	20	270±60	307			21.6±3.2	20	1.6±0.4	1
SR10	9.4±1.9	11	7.1±1.7	5			11.6±1.9	16	2.9±2.9	1
SR11	930±230	1068	6.5±1.6	7			84±11	105	1.9±1.4	3
SR12	330±70	370	39±9	42			15.5±2.1	17		
SR13	36±7	38	31±8	37			15.7±2.2	21		
SR14	25±5	31	23±5	27			5.3±0.8	8		
SR15	44±7	63	2.1±1.1	7			10.2±2.1	12		
SR16	39±8	38	1.7±0.9	2			27±4	40		
SR17	27±5	30	210±40	256			0.8±0.5	2		
SR18	14.8±3.2	15	85±14	104			17.8±2.4	24		
SR19	11.5±3.0	12	2.5±1.2	4			1.0±0.4	0		
SR20	11.8±2.6	14	3.0±1.5	3			17.8±3.0	30		
SR21	9.6±2.1	16	18.9±3.5	27			1.26±0.33	2		
SR22	10.0±1.6	15	15.9±2.8	18			830±180	955		
SR23	270±40	345	3.3±0.6	2			108±22	136		
SR24	143±20	169	4.4±1.6	2			117±26	139		
SR25	15.2±2.4	11	4.5±1.7	5			11.1±2.3	8		
SR26	13.8±3.4	18	8.2±2.2	8			111±24	128		
SR27	33±5	43	8.1±2.2	6			21±5	20		
SR28	29±4	38	9.7±2.1	12			42±10	45		
SR29	11.5±2.5	9	10.8±2.8	7			3.4±0.9	3		
SR30	6.7±1.2	5	1.1±0.4	3			320±50	408		
SR31	7.5±1.8	6	2.2±0.5	5			47±8	50		
SR32	5.9±1.0	14	2.6±0.5	3			51±9	62		
SR33	6.5±1.9	7	22±6	23			15.1±2.6	24		
SR34	6.7±1.2	11	7.2±1.4	8			131±24	157		
SR35	10.3±1.9	17	2.3±0.5	4			20±4	24		
SR36	8.6±1.7	11	0.42±0.33	1			27±5	36		
SR37	10.6±2.0	6	3.2±1.5	3			7.8±1.5	11		
SR38	7.3±1.3	5	1.4±0.6	0			12.9±2.6	18		
SR39	9.6±2.2	8	0.41±0.25	0			82±14	117		
SR40	9.2±1.9	11	3.1±0.7	7			18±4	26		
SR41	1.3±0.6	2	4±4	0			39±8	29		
SR42	0.6±0.4	1	4.7±0.9	8			4.9±0.9	7		
SR43	0.8±0.4	0	1.71±0.35	6			46±10	44		
SR44	0.7±0.4	1					5.7±1.2	11		
SR45	0.7±0.5	1								
SR46	42±7	59								
SR47	18±4	23								
SR48	13±9	10								
SR49	2.0±0.5	4								
SR50	6.3±1.0	13								
SR51	3.7±0.7	4								
SR52	1.26±0.33	4								
SR53	0.4±0.4	2								
SR54	10.1±1.5	24								
SR55	7.0±1.1	4								
SR56	4.3±0.9	5								
SR57	5.3±0.8	7								
SR58	6±6	6								
SR59	2.2±0.4	3								
SR60	1.8±0.5	5								
SR61	1.9±0.4	4								
SR62	1.3±0.9	0								

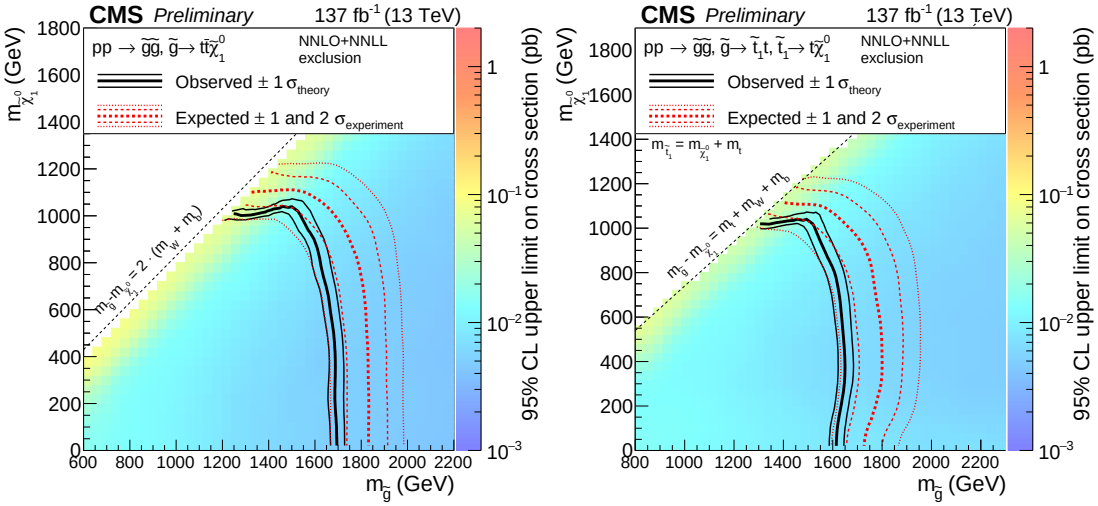

Figure 6: Exclusion regions at 95% CL in the $m_{\tilde{\chi}^0_1}$ versus $m_{\tilde{g}}$ plane for the T1tttt model (left), with off-shell third-generation squarks, and the T5tttt (right) model, with on-shell third-generation squarks. For the T5tttt model, $m_{\tilde{t}} - m_{\tilde{\chi}^0_1} = m_t$. The right-hand side color scale indicates the excluded cross section values for a given point in the SUSY particle mass plane. The solid, black curves represent the observed exclusion limits assuming the NLO+NLL cross sections [42–47] (thick line), or their variations of ± 1 standard deviation (thin lines). The dashed, red curves show the expected limits with the corresponding ± 1 and ± 2 standard deviation experimental uncertainties. Excluded regions are to the left and below the limit curves.

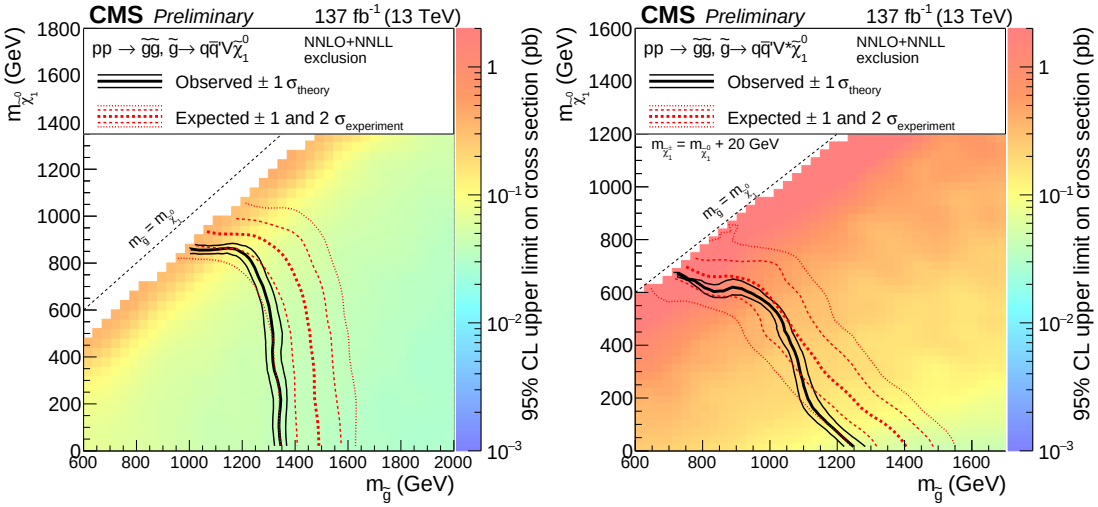

Figure 7: Exclusion regions at 95% CL in the plane of $m_{\tilde{\chi}^0_1}$ versus $m_{\tilde{g}}$ for the T5qqqqWZ model with $m_{\tilde{\chi}^\pm_1} = 0.5(m_{\tilde{g}} + m_{\tilde{\chi}^0_1})$ (a) and with $m_{\tilde{\chi}^\pm_1} = m_{\tilde{\chi}^0_1} + 20\,\text{GeV}$ (b). The notations are as in Fig. 6.

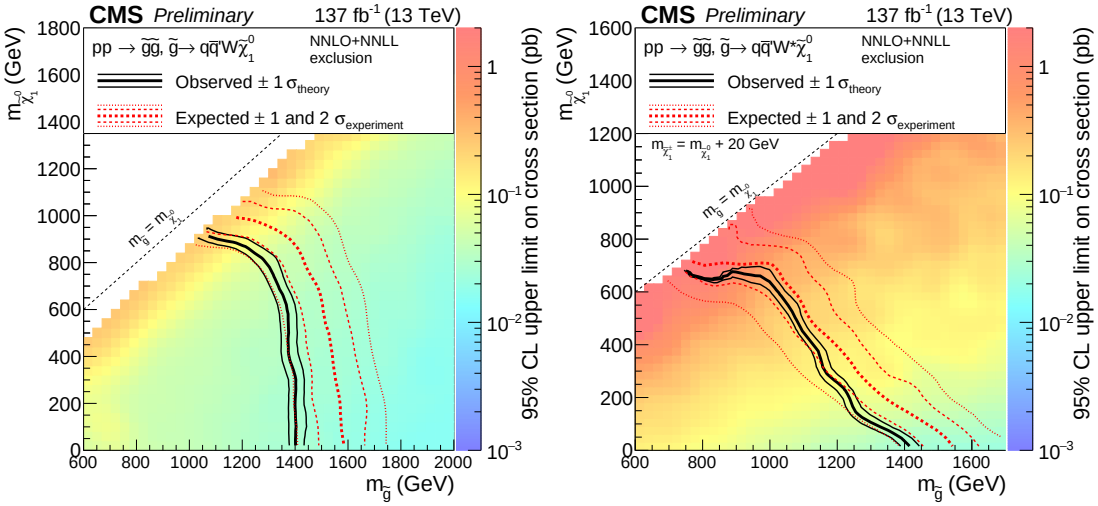

Figure 8: Exclusion regions at 95% CL in the plane of $m_{\tilde{\chi}_1^0}$ versus $m_{\tilde{g}}$ for the T5qqqqWW model with $m_{\tilde{\chi}_1^\pm} = 0.5(m_{\tilde{g}} + m_{\tilde{\chi}_1^0})$ (a) and with $m_{\tilde{\chi}_1^\pm} = m_{\tilde{\chi}_1^0} + 20\,\text{GeV}$ (b). The notations are as in Fig. 6.

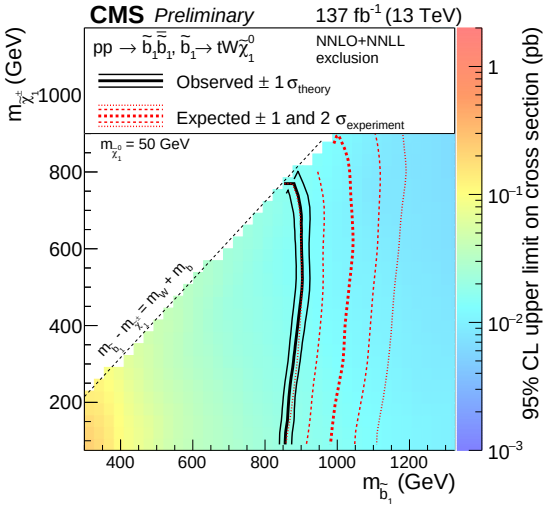

Figure 9: Exclusion regions at 95% CL in the plane of $m_{\tilde{\chi}_1^\pm}$ versus $m_{\tilde{b}}$ for the T6ttWW model with $m_{\tilde{\chi}_1^0} = 50\,\text{GeV}$. The notations are as in Fig. 6.

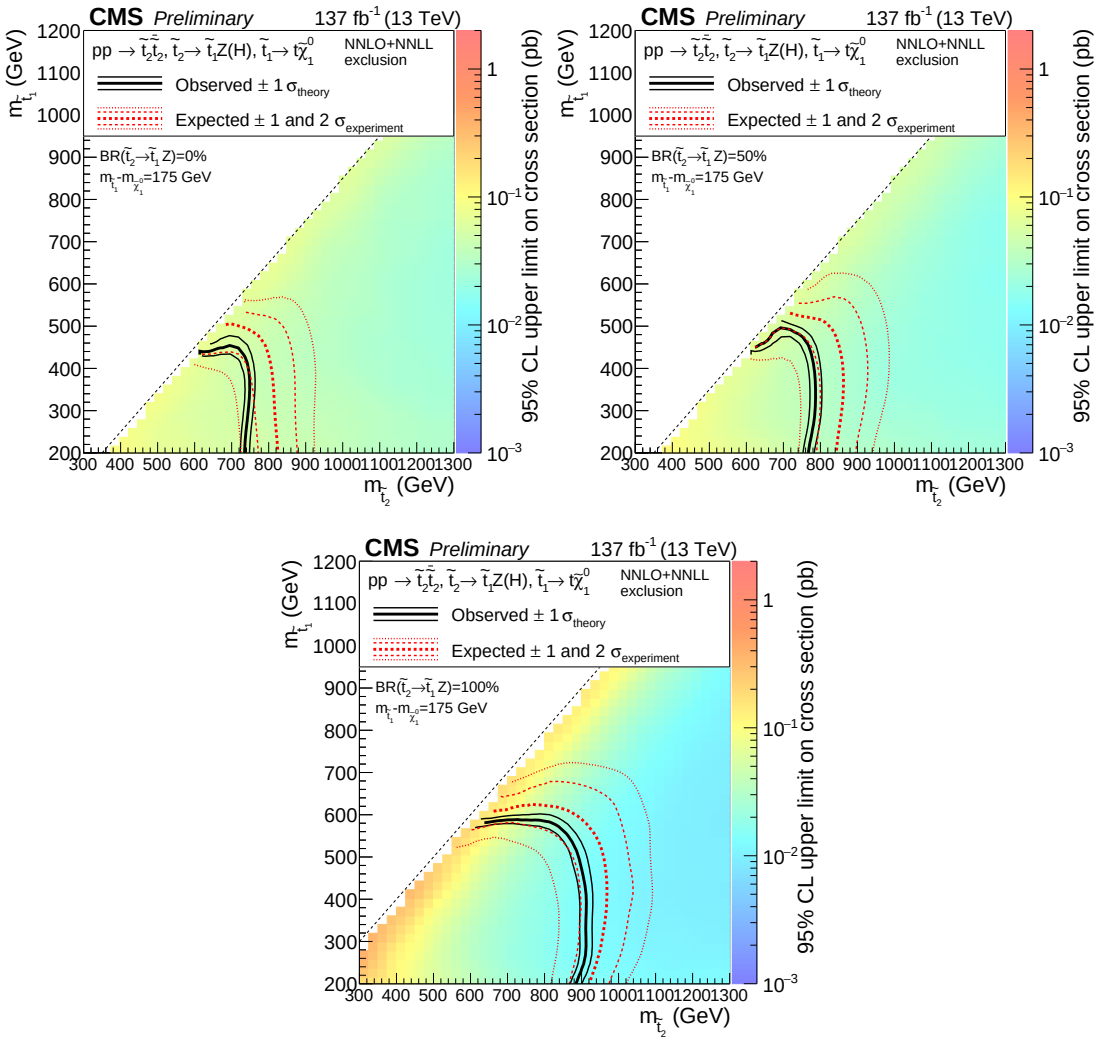

Figure 10: Exclusion regions at the 95% CL in the plane of $m(\tilde{t}_1)$ versus $m(\tilde{t}_2)$ for the T6ttHZ simplified model with $m(\tilde{t}_2) - m(\tilde{\chi}_1^0) = 175\,\text{GeV}$. The three exclusions represent $\text{BR}(\tilde{t}_2 \to \tilde{t}_1 Z)$ of 0%, 50%, and 100%, respectively. The right-hand side color scale indicates the excluded cross section values for a given point in the SUSY particle mass plane. Observed and expected limit curves indicate the boundaries of the excluded regions (to the left and below the curve).

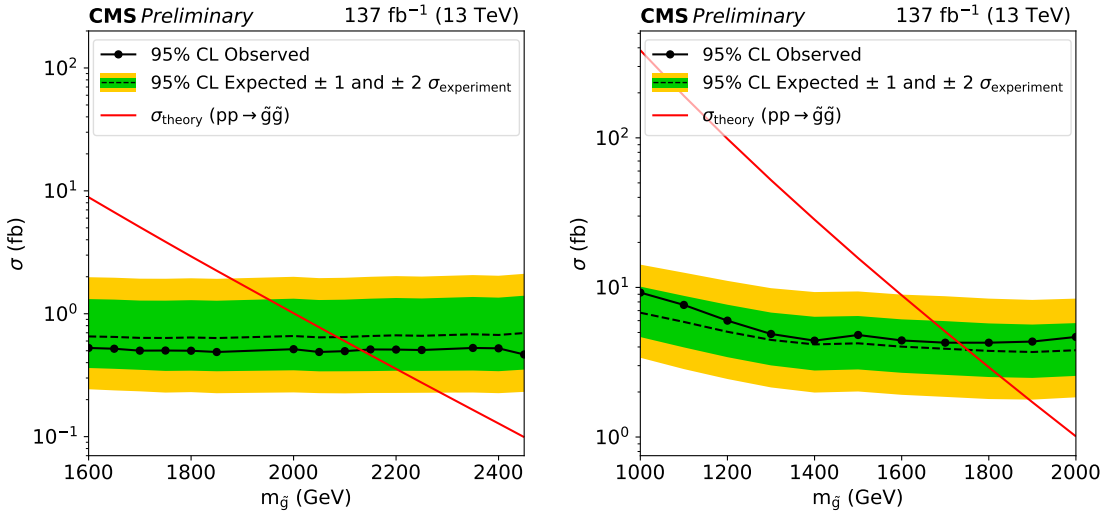

Figure 11: Limits on RPV gluino pair production with each gluino decaying into four quarks and one lepton (T1qqqqL, left) and each gluino decaying into a top, bottom, and strange quark (T1tbs, right)

8 Summary

A sample of same-sign dilepton or trilepton events produced in association with several jets in proton-proton collisions at 13 TeV, corresponding to an integrated luminosity of 137 fb^{-1}, has been studied to search for manifestations of physics beyond the standard model. The data are found to be consistent with the standard model expectations, and no excess event yield is observed. The results are interpreted as limits at 95% confidence level on cross sections for the production of new particles in simplified supersymmetric models, considering both RPC and RPV scenarios. Using calculations for these cross sections as functions of particle masses, the limits are turned into lower mass limits that are as high as 2.1 TeV for gluinos and 0.9 TeV for top and bottom squarks, depending on the details of the model.

References

[1] R. M. Barnett, J. F. Gunion, and H. E. Haber, "Discovering supersymmetry with like-sign dileptons", *Phys. Lett. B* **315** (1993) 349, doi:10.1016/0370-2693(93)91623-U, arXiv:hep-ph/9306204.

[2] M. Guchait and D. P. Roy, "Like-sign dilepton signature for gluino production at CERN LHC including top quark and Higgs boson effects", *Phys. Rev. D* **52** (1995) 133, doi:10.1103/PhysRevD.52.133, arXiv:hep-ph/9412329.

[3] Y. Bai and Z. Han, "Top-antitop and top-top resonances in the dilepton channel at the CERN LHC", *JHEP* **04** (2009) 056, doi:10.1088/1126-6708/2009/04/056, arXiv:0809.4487.

[4] E. L. Berger et al., "Top quark forward-backward asymmetry and same-sign top quark pairs", *Phys. Rev. Lett.* **106** (2011) 201801, doi:10.1103/PhysRevLett.106.201801, arXiv:1101.5625.

[5] T. Plehn and T. M. P. Tait, "Seeking Sgluons", *J. Phys. G* **36** (2009) 075001, doi:10.1088/0954-3899/36/7/075001, arXiv:0810.3919.

[6] S. Calvet, B. Fuks, P. Gris, and L. Valery, "Searching for sgluons in multitop events at a center-of-mass energy of 8 TeV", *JHEP* **04** (2013) 043, doi:10.1007/JHEP04(2013)043, arXiv:1212.3360.

[7] K. J. F. Gaemers and F. Hoogeveen, "Higgs production and decay into heavy flavors with the gluon fusion mechanism", *Phys. Lett. B* **146** (1984) 347, doi:10.1016/0370-2693(84)91711-8.

[8] G. C. Branco et al., "Theory and phenomenology of two-Higgs-doublet models", *Phys. Rept.* **516** (2012) 1, doi:10.1016/j.physrep.2012.02.002, arXiv:1106.0034.

[9] F. M. L. Almeida, Jr. et al., "Same-sign dileptons as a signature for heavy Majorana neutrinos in hadron-hadron collisions", *Phys. Lett. B* **400** (1997) 331, doi:10.1016/S0370-2693(97)00143-3, arXiv:hep-ph/9703441.

[10] R. Contino and G. Servant, "Discovering the top partners at the LHC using same-sign dilepton final states", *JHEP* **06** (2008) 026, doi:10.1088/1126-6708/2008/06/026, arXiv:0801.1679.

[11] ATLAS Collaboration, "Search for supersymmetry in final states with two same-sign or three leptons and jets using 36 fb^{-1} of $\sqrt{s} = 13$ TeV pp collision data with the ATLAS detector", *JHEP* **09** (2017) 084, doi:10.1007/JHEP09(2017)084, arXiv:1706.03731.

[12] CMS Collaboration, "Search for physics beyond the standard model in events with two leptons of same sign, missing transverse momentum, and jets in proton-proton collisions at $\sqrt{s} = 13$ TeV", *Eur. Phys. J.* **C77** (2017), no. 9, 578, doi:10.1140/epjc/s10052-017-5079-z, arXiv:1704.07323.

[13] CMS Collaboration, "Search for supersymmetry in events with at least three electrons or muons, jets, and missing transverse momentum in proton-proton collisions at $\sqrt{s} = 13$ TeV", *JHEP* **02** (2018) 067, doi:10.1007/JHEP02(2018)067, arXiv:1710.09154.

[14] P. Ramond, "Dual theory for free fermions", *Phys. Rev. D* **3** (1971) 2415, doi:10.1103/PhysRevD.3.2415.

[15] Y. A. Gol'fand and E. P. Likhtman, "Extension of the algebra of Poincaré group generators and violation of P invariance", *JETP Lett.* **13** (1971) 323.

[16] A. Neveu and J. H. Schwarz, "Factorizable dual model of pions", *Nucl. Phys. B* **31** (1971) 86, doi:10.1016/0550-3213(71)90448-2.

[17] D. V. Volkov and V. P. Akulov, "Possible universal neutrino interaction", *JETP Lett.* **16** (1972) 438.

[18] J. Wess and B. Zumino, "A lagrangian model invariant under supergauge transformations", *Phys. Lett. B* **49** (1974) 52, doi:10.1016/0370-2693(74)90578-4.

[19] J. Wess and B. Zumino, "Supergauge transformations in four-dimensions", *Nucl. Phys. B* **70** (1974) 39, doi:10.1016/0550-3213(74)90355-1.

[20] P. Fayet, "Supergauge invariant extension of the Higgs mechanism and a model for the electron and its neutrino", *Nucl. Phys. B* **90** (1975) 104, doi:10.1016/0550-3213(75)90636-7.

[21] H. P. Nilles, "Supersymmetry, supergravity and particle physics", *Phys. Rept.* **110** (1984) 1, doi:10.1016/0370-1573(84)90008-5.

[22] S. P. Martin, "A supersymmetry primer", in *Perspectives on Supersymmetry II*, G. L. Kane, ed., p. 1. World Scientific, 2010. Adv. Ser. Direct. High Energy Phys., vol. 21. doi:10.1142/9789814307505_0001.

[23] G. R. Farrar and P. Fayet, "Phenomenology of the production, decay, and detection of new hadronic states associated with supersymmetry", *Phys. Lett. B* **76** (1978) 575, doi:10.1016/0370-2693(78)90858-4.

[24] E. Nikolidakis and C. Smith, "Minimal Flavor Violation, Seesaw, and R-parity", *Phys. Rev.* **D77** (2008) 015021, doi:10.1103/PhysRevD.77.015021, arXiv:0710.3129.

[25] C. Smith, "Minimal Flavor Violation as an alternative to R-parity", in *Proceedings, 34th International Conference on High Energy Physics (ICHEP 2008): Philadelphia, Pennsylvania, July 30-August 5, 2008*. 2008. arXiv:0809.3152.

[26] C. Csaki, Y. Grossman, and B. Heidenreich, "MFV SUSY: A Natural Theory for R-Parity Violation", *Phys. Rev.* **D85** (2012) 095009, doi:10.1103/PhysRevD.85.095009, arXiv:1111.1239.

[27] J. Alwall et al., "The automated computation of tree-level and next-to-leading order differential cross sections, and their matching to parton shower simulations", *JHEP* **07** (2014) 079, doi:10.1007/JHEP07(2014)079, arXiv:1405.0301.

[28] J. Alwall et al., "Comparative study of various algorithms for the merging of parton showers and matrix elements in hadronic collisions", *Eur. Phys. J. C* **53** (2008) 473, doi:10.1140/epjc/s10052-007-0490-5, arXiv:0706.2569.

[29] R. Frederix and S. Frixione, "Merging meets matching in MC@NLO", *JHEP* **12** (2012) 061, doi:10.1007/JHEP12(2012)061, arXiv:1209.6215.

[30] T. Melia, P. Nason, R. Rontsch, and G. Zanderighi, "W^+W^-, WZ and ZZ production in the POWHEG BOX", *JHEP* **11** (2011) 078, doi:10.1007/JHEP11(2011)078, arXiv:1107.5051.

[31] P. Nason and G. Zanderighi, "W^+W^- , WZ and ZZ production in the POWHEG BOX V2", *Eur. Phys. J. C* **74** (2014) 2702, doi:10.1140/epjc/s10052-013-2702-5, arXiv:1311.1365.

[32] NNPDF Collaboration, "Parton distributions for the LHC Run II", *JHEP* **04** (2015) 040, doi:10.1007/JHEP04(2015)040, arXiv:1410.8849.

[33] NNPDF Collaboration, "Parton distributions from high-precision collider data", *Eur. Phys. J.* **C77** (2017), no. 10, 663, doi:10.1140/epjc/s10052-017-5199-5, arXiv:1706.00428.

[34] T. Sjöstrand et al., "An Introduction to PYTHIA 8.2", *Comput. Phys. Commun.* **191** (2015) 159–177, doi:10.1016/j.cpc.2015.01.024, arXiv:1410.3012.

[35] P. Skands, S. Carrazza, and J. Rojo, "Tuning PYTHIA 8.1: the Monash 2013 tune", *Eur. Phys. J. C* **74** (2014) 3024, doi:10.1140/epjc/s10052-014-3024-y, arXiv:1404.5630.

[36] CMS Collaboration, "Event generator tunes obtained from underlying event and multiparton scattering measurements", *Eur. Phys. J. C* **76** (2016) 155, doi:10.1140/epjc/s10052-016-3988-x, arXiv:1512.00815.

[37] CMS Collaboration, "Extraction and validation of a new set of CMS PYTHIA8 tunes from underlying-event measurements", Technical Report CMS-PAS-GEN-17-001, CERN, Geneva, 2018.

[38] GEANT4 Collaboration, "GEANT4 — a simulation toolkit", *Nucl. Instrum. Meth. A* **506** (2003) 250, doi:10.1016/S0168-9002(03)01368-8.

[39] S. Abdullin et al., "The fast simulation of the CMS detector at LHC", *J. Phys. Conf. Ser.* **331** (2011) 032049, doi:10.1088/1742-6596/331/3/032049.

[40] CMS Collaboration, "Measurements of $t\bar{t}$ cross sections in association with b jets and inclusive jets and their ratio using dilepton final states in pp collisions at $\sqrt{s}$ = 13 TeV", *Phys. Lett.* **B776** (2018) 355–378, doi:10.1016/j.physletb.2017.11.043, arXiv:1705.10141.

[41] W. Beenakker et al., "NNLL-fast: predictions for coloured supersymmetric particle production at the LHC with threshold and Coulomb resummation", *JHEP* **12** (2016) 133, doi:10.1007/JHEP12(2016)133, arXiv:1607.07741.

[42] W. Beenakker, R. Höpker, M. Spira, and P. M. Zerwas, "Squark and gluino production at hadron colliders", *Nucl. Phys. B* **492** (1997) 51, doi:10.1016/S0550-3213(97)80027-2, arXiv:hep-ph/9610490.

[43] A. Kulesza and L. Motyka, "Threshold resummation for squark-antisquark and gluino-pair production at the LHC", *Phys. Rev. Lett.* **102** (2009) 111802, doi:10.1103/PhysRevLett.102.111802, arXiv:0807.2405.

[44] A. Kulesza and L. Motyka, "Soft gluon resummation for the production of gluino-gluino and squark-antisquark pairs at the LHC", *Phys. Rev. D* **80** (2009) 095004, doi:10.1103/PhysRevD.80.095004, arXiv:0905.4749.

[45] W. Beenakker et al., "Soft-gluon resummation for squark and gluino hadroproduction", *JHEP* **12** (2009) 041, doi:10.1088/1126-6708/2009/12/041, arXiv:0909.4418.

[46] W. Beenakker et al., "Squark and gluino hadroproduction", *Int. J. Mod. Phys. A* **26** (2011) 2637, doi:10.1142/S0217751X11053560, arXiv:1105.1110.

[47] C. Borschensky et al., "Squark and gluino production cross sections in pp collisions at $\sqrt{s}$ = 13, 14, 33 and 100 TeV", *Eur. Phys. J. C* **74** (2014) 3174, doi:10.1140/epjc/s10052-014-3174-y, arXiv:1407.5066.

[48] D. Alves et al., "Simplified models for LHC new physics searches", *J. Phys. G* **39** (2012) 105005, doi:10.1088/0954-3899/39/10/105005, arXiv:1105.2838.

[49] CMS Collaboration, "Interpretation of searches for supersymmetry with simplified models", *Phys. Rev. D* **88** (2013) 052017, doi:10.1103/PhysRevD.88.052017, arXiv:1301.2175.

[50] CMS Collaboration, "The CMS experiment at the CERN LHC", *JINST* **3** (2008) S08004, doi:10.1088/1748-0221/3/08/S08004.

[51] CMS Collaboration, "The CMS trigger system", *JINST* **12** (2017) P01020, doi:10.1088/1748-0221/12/01/P01020, arXiv:1609.02366.

[52] CMS Collaboration, "Particle-flow reconstruction and global event description with the cms detector", *JINST* **12** (2017) P10003, doi:10.1088/1748-0221/12/10/P10003, arXiv:1706.04965.

[53] CMS Collaboration, "Performance of electron reconstruction and selection with the CMS detector in proton-proton collisions at $\sqrt{s}$ = 8 TeV", *JINST* **10** (2015) P06005, doi:10.1088/1748-0221/10/06/P06005, arXiv:1502.02701.

[54] CMS Collaboration, "Performance of CMS muon reconstruction in pp collision events at sqrt(s) = 7 TeV", *JINST* **7** (2012) P10002, doi:10.1088/1748-0221/7/10/P10002, arXiv:1206.4071.

[55] M. Cacciari, G. P. Salam, and G. Soyez, "The anti-k_t jet clustering algorithm", *JHEP* **04** (2008) 063, doi:10.1088/1126-6708/2008/04/063, arXiv:0802.1189.

[56] M. Cacciari, G. P. Salam, and G. Soyez, "FastJet user manual", *Eur. Phys. J. C* **72** (2012) 1896, doi:10.1140/epjc/s10052-012-1896-2, arXiv:1111.6097.

[57] CMS Collaboration, "Jet energy scale and resolution in the CMS experiment in pp collisions at 8 TeV", *JINST* **12** (2016) P02014, doi:10.1088/1748-0221/12/02/P02014, arXiv:1607.03663.

[58] CMS Collaboration, "Jet algorithms performance in 13 TeV data", CMS Physics Analysis Summary CMS-PAS-JME-16-003, 2017.

[59] CMS Collaboration, "Identification of heavy-flavour jets with the CMS detector in pp collisions at 13 TeV", *JINST* **13** (2018), no. 05, P05011, doi:10.1088/1748-0221/13/05/P05011, arXiv:1712.07158.

[60] CMS Collaboration, "Performance of missing transverse momentum in pp collisions at sqrt(s)=13 TeV using the CMS detector", CMS Physics Analysis Summary CMS-PAS-JME-17-001, 2018.

[61] CMS Collaboration, "Search for new physics in same-sign dilepton events in proton-proton collisions at $\sqrt{s} = 13$ TeV", *Eur. Phys. J. C* **76** (2016) 439, doi:10.1140/epjc/s10052-016-4261-z, arXiv:1605.03171.

[62] CMS Collaboration, "Determination of jet energy calibration and transverse momentum resolution in CMS", *JINST* **6** (2011) P11002, doi:10.1088/1748-0221/6/11/P11002, arXiv:1107.4277.

[63] CMS Collaboration, "Performance of the CMS missing transverse momentum reconstruction in pp data at $\sqrt{s}$ = 8 TeV", *JINST* **10** (2015) P02006, doi:10.1088/1748-0221/10/02/P02006, arXiv:1411.0511.

[64] CMS Collaboration, "CMS Luminosity Measurements for the 2016 Data Taking Period", CMS Physics Analysis Summary CMS-PAS-LUM-17-001, 2017.

[65] CMS Collaboration, "Measurement of the inelastic proton-proton cross section at $\sqrt{s} = 13$ TeV", *JHEP* **07** (2018) 161, doi:10.1007/JHEP07(2018)161, arXiv:1802.02613.

[66] A. Kalogeropoulos and J. Alwall, "The SysCalc code: A tool to derive theoretical systematic uncertainties", arXiv:1801.08401.

[67] ATLAS Collaboration, "Measurement of the $t\bar{t}Z$ and $t\bar{t}W$ cross sections in proton-proton collisions at $\sqrt{s} = 13$ TeV with the ATLAS detector", arXiv:1901.03584.

[68] CMS Collaboration, "Measurement of the cross section for top quark pair production in association with a W or Z boson in proton-proton collisions at $\sqrt{s} = 13$ TeV", *JHEP* **08** (2018) 011, doi:10.1007/JHEP08(2018)011, arXiv:1711.02547.

[69] T. Junk, "Confidence level computation for combining searches with small statistics", *Nucl. Instrum. Meth. A* **434** (1999) 435, doi:10.1016/S0168-9002(99)00498-2, arXiv:hep-ex/9902006.

[70] A. L. Read, "Presentation of search results: the CL_S technique", *J. Phys. G* **28** (2002) 2693, doi:10.1088/0954-3899/28/10/313.

[71] ATLAS and CMS Collaborations, "Procedure for the lhc higgs boson search combination in summer 2011", ATL-PHYS-PUB-2011-011, CMS NOTE-2011/005, 2011.

[72] G. Cowan, K. Cranmer, E. Gross, and O. Vitells, "Asymptotic formulae for likelihood-based tests of new physics", *Eur. Phys. J. C* **71** (2011) 1554, doi:10.1140/epjc/s10052-011-1554-0, arXiv:1007.1727. [Erratum: doi:10.1140/epjc/s10052-013-2501-z.

A Detailed Results

Tables 9-13, corresponding to Figures 4-5, show background predictions per process within each signal region.

Table 9: Event yields in HH regions. Yields shown as "-" have a contribution smaller than 0.01, or do not contribute to a particular region.

	$t\bar{t}W$	$t\bar{t}Z$	$t\bar{t}H$	WZ	WW	X+γ	Rares	Charge misid.	Nonprompt lep.	SM expected	Data
SR1	53±14	14.2±3.5	14±4	350±90	128±30	260±140	100±50	125±13	460±220	1510±310	1609
SR2	29±7	7.8±2.0	7.8±2.1	122±32	160±40	90±40	38±19	31.6±3.3	100±50	590±90	647
SR3	8.1±2.1	1.5±0.4	1.6±0.4	20±5	12.9±3.1	9±8	9±4	13.6±1.5	27±17	103±22	132
SR4	6.1±1.6	2.3±0.6	3.4±0.9	4.0±1.1	4.3±1.0	0.33±0.17	4.3±2.2	1.83±0.19	12±6	38±7	51
SR5	4.0±1.0	0.46±0.12	0.49±0.13	16±4	21±5	6±6	4.8±2.6	0.47±0.05	4.3±2.0	57±10	49
SR6	1.7±0.4	0.48±0.13	0.56±0.15	6.8±1.9	5.1±1.3	9±7	2.5±1.3	0.56±0.06	5.4±2.7	32±9	23
SR7	0.90±0.24	0.26±0.07	0.37±0.10	0.80±0.23	0.84±0.20	1.2±1.2	0.40±0.21	0.08±0.01	0.7±0.4	5.5±1.7	7
SR8	1.7±0.4	0.27±0.08	0.23±0.06	2.8±0.8	6.8±1.6	5±5	1.9±1.0	3.9±0.4	2.6±1.6	25±6	31
SR9	1.00±0.26	0.27±0.08	0.20±0.06	2.7±0.8	4.5±1.1	4.1±3.5	1.1±0.6	4.4±0.5	2.2±1.6	21±5	20
SR10	1.4±0.4	0.27±0.07	0.27±0.08	0.84±0.24	2.7±0.7	0.02±0.02	1.6±0.9	0.62±0.07	1.7±0.8	9.4±1.9	11
SR11	130±34	34±8	35±10	30±8	11.1±2.7	47±22	30±16	82±9	530±220	930±230	1068
SR12	79±20	21±5	22±6	14±4	16±4	18±10	16±8	20.0±2.1	120±60	330±70	370
SR13	12.8±3.3	2.0±0.5	2.0±0.5	1.4±0.4	0.74±0.22	1.4±1.1	1.3±0.7	3.6±0.4	11±6	36±7	38
SR14	6.4±1.7	1.9±0.5	2.0±0.5	0.41±0.18	0.30±0.12	1.1±0.7	1.0±0.5	3.9±0.4	8±5	25±5	31
SR15	13.8±3.5	4.0±1.0	6.4±1.7	0.51±0.17	0.68±0.16	0.6±0.4	3.5±1.7	1.06±0.11	13±6	44±7	63
SR16	7.8±2.0	3.9±1.0	6.2±1.7	0.41±0.13	0.35±0.08	0.8±0.5	2.7±1.4	1.13±0.12	15±7	39±8	38
SR17	9.2±2.4	1.20±0.29	1.4±0.4	1.7±0.5	1.9±0.5	3.3±3.3	1.7±0.8	0.82±0.08	6.3±3.0	27±5	30
SR18	4.0±1.0	1.02±0.25	1.28±0.35	0.89±0.28	0.51±0.13	0.8±0.4	0.9±0.5	0.86±0.09	4.6±2.8	14.8±3.2	15
SR19	2.7±0.7	0.87±0.21	1.23±0.34	0.24±0.07	0.16±0.04	1.6±1.5	0.8±0.4	0.18±0.02	3.7±1.8	11.5±3.0	12
SR20	4.9±1.3	0.76±0.19	0.60±0.16	0.49±0.16	0.64±0.15	1.7±1.7	0.7±0.4	1.12±0.12	0.9±0.9	11.8±2.6	14
SR21	2.7±0.7	0.71±0.18	0.59±0.16	0.26±0.13	0.62±0.15	0.63±0.30	0.63±0.33	1.18±0.13	2.3±1.8	9.6±2.1	16
SR22	4.4±1.2	0.76±0.18	1.00±0.27	0.13±0.05	0.31±0.08	0.44±0.27	1.3±0.7	0.46±0.05	1.1±0.9	10.0±1.6	15
SR23	77±20	20±5	22±6	1.7±0.5	0.58±0.15	22±11	9±5	53±6	64±31	270±40	345
SR24	55±14	14.8±3.5	17±5	1.02±0.34	0.83±0.23	9±4	8±4	12.7±1.3	25±13	143±20	169
SR25	7.5±2.0	1.06±0.25	1.18±0.34	0.07±0.02	-	0.6±0.4	0.8±0.4	2.12±0.23	1.9±1.4	15.2±2.4	11
SR26	4.0±1.1	0.89±0.23	1.3±0.4	0.02±0.01	0.02±0.01	2.9±2.8	0.52±0.28	2.01±0.22	2.1±1.4	13.8±3.4	18
SR27	12.1±3.1	3.7±0.9	6.0±1.7	0.15±0.06	0.05±0.02	0.9±0.6	3.9±2.0	0.90±0.09	5.1±2.2	33±5	43
SR28	7.4±1.9	3.5±0.9	6.0±1.7	-	0.13±0.04	1.0±0.5	3.3±1.7	0.97±0.10	6.5±2.8	29±4	38
SR29	5.4±1.4	0.62±0.15	0.78±0.22	0.12±0.06	0.06±0.03	0.18±0.10	0.58±0.31	0.38±0.04	3.4±2.2	11.5±2.5	9
SR30	2.7±0.7	0.57±0.14	0.80±0.22	0.17±0.06	0.08±0.02	0.45±0.27	0.37±0.20	0.45±0.05	1.1±0.8	6.7±1.2	5
SR31	2.7±0.7	0.56±0.13	1.13±0.32	0.13±0.06	0.07±0.02	0.14±0.07	1.1±0.6	0.15±0.02	1.5±1.4	7.5±1.8	6
SR32	3.4±0.9	0.60±0.15	0.46±0.13	-	0.05±0.01	0.34±0.20	0.38±0.20	0.54±0.06	0.10±0.10	5.9±1.0	14
SR33	2.1±0.5	0.59±0.14	0.57±0.16	-	0.01±0.01	0.24±0.15	0.27±0.14	0.54±0.06	2.2±1.8	6.5±1.9	7
SR34	2.9±0.8	0.66±0.17	0.81±0.23	-	0.08±0.03	0.22±0.11	1.1±0.6	0.31±0.03	0.6±0.5	6.7±1.2	11
SR35	3.2±0.9	0.85±0.22	1.17±0.34	-	-	0.23±0.13	0.55±0.30	0.93±0.10	3.3±1.5	10.3±1.9	17
SR36	1.8±0.5	0.79±0.20	1.21±0.35	-	-	0.5±0.4	0.51±0.27	0.92±0.10	2.9±1.5	8.6±1.7	11
SR37	3.3±0.9	0.96±0.24	1.10±0.32	-	0.02±0.01	0.40±0.22	1.0±0.5	0.55±0.06	3.3±1.6	10.6±2.0	6
SR38	1.9±0.5	0.86±0.22	1.06±0.31	-	-	0.35±0.28	0.9±0.5	0.55±0.06	1.6±0.9	7.3±1.3	5
SR39	2.2±0.6	0.65±0.17	1.16±0.35	0.02±0.01	-	0.23±0.11	3.5±1.8	0.19±0.02	1.7±1.0	9.6±2.2	8
SR40	1.5±0.4	0.82±0.23	1.3±0.4	-	-	0.29±0.16	3.1±1.6	0.20±0.02	2.0±1.0	9.2±1.9	11
SR41	0.43±0.16	0.14±0.05	0.16±0.06	-	-	0.07±0.07	0.13±0.07	0.14±0.02	0.20±0.20	1.3±0.6	2
SR42	0.24±0.08	0.08±0.06	0.08±0.03	-	-	0.03±0.03	0.17±0.09	0.04±0.01	-	0.6±0.4	1
SR43	0.20±0.07	0.04±0.04	0.07±0.03	-	-	0.12±0.12	0.13±0.07	0.04±0.01	0.24±0.24	0.8±0.4	0
SR44	0.14±0.09	0.03±0.03	0.08±0.03	-	-	0.02±0.02	0.38±0.21	0.04±0.01	0.04±0.04	0.7±0.4	1
SR45	0.15±0.06	0.04±0.03	0.07±0.03	0.03±0.03	-	0.04±0.04	0.32±0.18	0.02±0.01	-	0.7±0.5	1
SR46	9.5±2.5	0.90±0.22	0.90±0.24	8.0±2.1	14.6±3.5	2.3±2.3	3.6±1.9	0.51±0.05	1.7±1.5	42±7	59
SR47	3.4±0.9	0.86±0.23	0.91±0.24	2.9±0.8	2.9±0.7	1.8±1.8	1.5±0.8	0.60±0.06	2.9±1.6	18±4	23
SR48	1.3±0.4	0.11±0.05	0.05±0.03	1.6±0.6	4.5±1.1	4±4	0.4±0.4	0.05±0.02	0.4±0.4	13±9	10
SR49	0.37±0.10	0.14±0.04	0.08±0.02	0.56±0.20	0.40±0.11	0.02±0.01	0.34±0.21	0.04±0.00	0.03±0.03	2.0±0.5	4
SR50	2.5±0.7	0.28±0.08	0.54±0.16	0.33±0.11	0.72±0.20	0.07±0.03	1.1±0.6	0.08±0.01	0.67±0.30	6.3±1.0	13
SR51	1.13±0.31	0.34±0.11	0.56±0.17	0.17±0.06	0.15±0.05	0.02±0.01	0.8±0.4	0.08±0.01	0.40±0.35	3.7±0.7	4
SR52	0.45±0.12	0.06±0.02	0.05±0.02	0.27±0.12	0.15±0.04	0.02±0.01	0.20±0.11	-	0.05±0.05	1.26±0.33	4
SR53	0.19±0.08	0.04±0.04	0.06±0.03	-	0.03±0.03	-	0.07±0.04	0.01±0.01	-	0.4±0.4	2
SR54	1.7±0.4	0.24±0.07	0.23±0.07	1.07±0.31	4.5±1.1	0.7±0.6	0.64±0.32	0.36±0.04	0.69±0.35	10.1±1.5	24
SR55	0.97±0.25	0.15±0.05	0.12±0.04	0.72±0.21	3.8±0.9	0.03±0.03	0.57±0.31	0.31±0.04	0.33±0.31	7.0±1.1	4
SR56	0.57±0.15	0.04±0.01	0.06±0.02	0.45±0.16	2.4±0.6	0.34±0.34	0.17±0.09	0.18±0.02	0.15±0.10	4.3±0.9	5
SR57	2.0±0.5	0.49±0.12	0.53±0.17	0.22±0.07	0.48±0.13	0.04±0.02	0.7±0.4	0.22±0.02	0.6±0.5	5.3±0.8	7
SR58	1.6±0.5	0.16±0.08	0.30±0.10	0.12±0.12	0.47±0.15	2.0±2.0	0.7±0.6	0.13±0.02	0.4±0.4	6±6	6
SR59	1.01±0.30	0.06±0.02	0.15±0.06	0.15±0.06	0.37±0.09	-	0.25±0.16	0.12±0.01	0.11±0.11	2.2±0.4	3
SR60	0.59±0.17	0.09±0.04	0.33±0.10	-	0.01±0.01	0.03±0.02	0.7±0.4	0.04±0.00	0.06±0.06	1.8±0.5	5
SR61	0.66±0.18	0.11±0.03	0.20±0.06	0.08±0.05	0.09±0.02	-	0.52±0.26	0.02±0.00	0.25±0.15	1.9±0.4	4
SR62	0.38±0.13	0.05±0.05	0.14±0.05	0.03±0.03	0.03±0.03	0.01±0.01	0.22±0.15	0.02±0.01	0.4±0.4	1.3±0.9	0

Table 10: Event yields in HL regions. Yields shown as "-" have a contribution smaller than 0.01, or do not contribute to a particular region.

	$t\bar{t}W$	$t\bar{t}Z$	$t\bar{t}H$	W Z	WW	X+γ	Rares	Charge misid.	Nonprompt lep.	SM expected	Data
SR1	17±4	6.1±1.5	6.7±1.8	170±40	48±11	160±80	50±26	29.8±3.2	820±280	1300±310	1504
SR2	7.2±1.9	2.6±0.6	3.2±0.9	36±10	46±11	32±20	11±6	5.8±0.6	170±60	310±70	319
SR3	0.95±0.25	0.20±0.06	0.32±0.08	4.7±1.2	2.2±0.6	0.13±0.13	1.8±0.9	0.20±0.02	14±5	25±6	32
SR4	1.8±0.5	0.81±0.20	1.7±0.5	1.04±0.32	1.41±0.33	0.22±0.15	1.2±0.6	0.41±0.04	23±8	32±8	32
SR5	1.14±0.30	0.21±0.05	0.22±0.06	5.5±1.5	7.5±1.9	4±4	1.1±0.6	0.09±0.01	9.0±3.3	29±6	32
SR6	0.33±0.08	0.23±0.07	0.22±0.06	2.3±0.6	1.4±0.4	3.4±3.4	0.46±0.28	0.18±0.02	8.8±3.1	17±6	11
SR7	0.24±0.10	0.09±0.08	0.18±0.05	0.25±0.18	0.23±0.12	0.25±0.25	0.32±0.32	0.02±0.00	3.0±1.8	4.5±2.5	6
SR8	45±12	16±4	18±5	14±4	3.3±0.8	34±17	13±7	22.7±2.3	850±250	1010±250	1223
SR9	22±6	8.1±1.9	9.8±2.7	4.8±1.3	4.2±1.0	6.0±3.4	4.4±2.3	4.0±0.4	210±60	270±60	307
SR10	1.6±0.4	0.25±0.06	0.34±0.10	0.10±0.04	0.16±0.05	0.61±0.34	0.20±0.13	0.21±0.02	3.6±1.4	7.1±1.7	5
SR11	0.79±0.21	0.23±0.06	0.40±0.11	0.08±0.04	0.05±0.02	0.16±0.09	0.20±0.09	0.17±0.02	4.4±1.6	6.5±1.6	7
SR12	4.1±1.1	1.22±0.30	3.2±0.9	0.18±0.07	0.24±0.08	1.6±1.1	0.8±0.4	0.25±0.03	27±9	39±9	42
SR13	1.9±0.5	1.36±0.33	3.1±0.9	0.09±0.06	0.06±0.02	1.1±0.5	0.9±0.5	0.29±0.03	22±7	31±8	37
SR14	4.3±1.1	0.86±0.21	1.12±0.31	1.3±0.4	0.87±0.21	0.48±0.26	0.57±0.30	0.38±0.04	13±5	23±5	27
SR15	0.61±0.18	0.08±0.08	0.29±0.09	-	0.04±0.04	0.04±0.04	0.12±0.07	0.02±0.01	0.9±0.9	2.1±1.1	7
SR16	0.27±0.10	0.16±0.08	0.34±0.11	0.04±0.04	0.01±0.01	-	0.12±0.07	0.02±0.01	0.8±0.8	1.7±0.9	2
SR17	29±7	10.1±2.4	11.6±3.3	0.58±0.19	0.09±0.03	17±8	4.0±2.1	16.1±1.7	130±40	210±40	256
SR18	17±4	6.2±1.5	7.8±2.2	0.49±0.14	0.23±0.06	5.8±2.7	2.3±1.2	3.04±0.32	42±13	85±14	104
SR19	0.72±0.23	0.12±0.06	0.27±0.08	-	-	0.03±0.03	0.05±0.05	0.12±0.02	1.2±0.9	2.5±1.2	4
SR20	0.56±0.16	0.12±0.05	0.25±0.08	0.05±0.05	0.03±0.03	0.13±0.10	0.09±0.06	0.13±0.02	1.6±1.5	3.0±1.5	3
SR21	4.2±1.1	1.6±0.4	3.1±0.9	-	0.10±0.03	2.5±2.1	1.2±0.6	0.22±0.02	5.9±1.9	18.9±3.5	27
SR22	2.0±0.5	1.35±0.32	3.1±0.9	-	-	0.8±0.5	0.9±0.5	0.22±0.02	7.5±2.6	15.9±2.8	18
SR23	1.9±0.5	0.20±0.06	0.42±0.12	0.02±0.02	0.09±0.04	0.20±0.10	0.17±0.09	0.10±0.01	0.17±0.16	3.3±0.6	2
SR24	0.82±0.22	0.27±0.10	0.35±0.11	0.17±0.17	0.01±0.01	0.12±0.12	0.14±0.08	0.13±0.02	2.4±1.3	4.4±1.6	2
SR25	1.05±0.30	0.26±0.10	0.56±0.17	-	-	0.20±0.20	0.27±0.15	0.04±0.01	2.1±1.4	4.5±1.7	5
SR26	0.99±0.28	0.41±0.10	0.60±0.18	-	0.01±0.00	0.46±0.23	0.18±0.10	0.25±0.03	5.3±2.2	8.2±2.2	8
SR27	0.49±0.14	0.47±0.12	0.58±0.17	-	-	0.50±0.23	0.16±0.09	0.24±0.03	5.7±2.1	8.1±2.2	6
SR28	1.4±0.4	0.60±0.16	1.13±0.33	-	-	0.22±0.10	1.0±0.5	0.14±0.02	5.2±2.0	9.7±2.1	12
SR29	0.88±0.23	0.42±0.10	1.10±0.33	-	-	0.32±0.17	1.0±0.5	0.19±0.02	6.9±2.6	10.8±2.8	7
SR30	0.36±0.10	0.14±0.04	0.19±0.06	-	-	0.02±0.01	0.30±0.16	0.04±0.00	0.05±0.05	1.1±0.4	3
SR31	0.39±0.11	0.05±0.02	0.16±0.05	0.14±0.05	0.12±0.05	0.04±0.03	0.08±0.05	0.08±0.01	1.1±0.4	2.2±0.5	5
SR32	0.73±0.20	0.05±0.02	0.18±0.05	0.16±0.08	0.31±0.10	0.07±0.03	0.32±0.17	0.07±0.01	0.73±0.33	2.6±0.5	3
SR33	2.5±0.6	0.32±0.08	0.32±0.09	2.6±0.7	4.9±1.2	5±5	1.6±0.8	0.11±0.01	4.7±1.4	22±6	23
SR34	0.96±0.24	0.24±0.06	0.29±0.08	1.3±0.4	0.70±0.19	0.08±0.06	0.7±0.4	0.09±0.01	2.8±1.1	7.2±1.4	8
SR35	0.29±0.08	0.03±0.01	0.02±0.01	0.61±0.17	0.93±0.28	0.02±0.01	0.12±0.10	-	0.27±0.27	2.3±0.5	4
SR36	0.11±0.04	0.03±0.02	-	0.04±0.04	0.06±0.05	-	0.08±0.08	-	0.09±0.09	0.42±0.33	1
SR37	0.72±0.22	0.12±0.06	0.20±0.06	0.12±0.12	0.34±0.12	0.02±0.02	0.20±0.13	0.02±0.01	1.4±1.3	3.2±1.5	3
SR38	0.19±0.09	0.11±0.06	0.20±0.07	0.02±0.02	0.05±0.04	0.01±0.01	0.16±0.11	0.02±0.01	0.6±0.5	1.4±0.6	0
SR39	0.21±0.09	0.02±0.02	0.03±0.01	-	0.07±0.04	-	0.04±0.03	-	0.05±0.05	0.41±0.25	0
SR40	0.57±0.15	0.06±0.03	0.18±0.06	0.07±0.07	0.95±0.25	-	0.26±0.13	0.03±0.00	1.0±0.6	3.1±0.7	7
SR41	0.25±0.11	0.11±0.06	0.18±0.07	0.04±0.04	0.17±0.09	2.1±2.1	0.13±0.09	0.03±0.01	1.1±0.9	4±4	0
SR42	0.87±0.24	0.11±0.03	0.15±0.05	0.26±0.08	1.5±0.4	0.03±0.01	0.23±0.12	0.06±0.01	1.4±0.7	4.7±0.9	8
SR43	0.24±0.07	0.12±0.04	0.21±0.07	0.22±0.08	0.31±0.08	0.02±0.01	0.18±0.10	0.07±0.01	0.35±0.22	1.71±0.35	6

Table 11: Event yields in LL regions. Yields shown as "-" have a contribution smaller than 0.01, or do not contribute to a particular region.

	$t\bar{t}W$	$t\bar{t}Z$	$t\bar{t}H$	W Z	WW	X+γ	Rares	Charge misid.	Nonprompt lep.	SM expected	Data
SR1	0.32±0.08	0.26±0.07	0.30±0.08	1.6±0.5	2.2±0.5	0.09±0.09	0.39±0.19	0.05±0.01	14±6	20±6	25
SR2	0.09±0.03	0.04±0.02	0.06±0.02	1.11±0.34	0.86±0.21	0.03±0.01	0.37±0.19	-	2.3±1.4	4.9±1.5	6
SR3	0.98±0.24	0.86±0.21	1.01±0.28	0.22±0.07	0.13±0.03	0.21±0.21	0.29±0.16	0.07±0.01	19±6	23±6	29
SR4	0.45±0.14	0.10±0.04	0.27±0.08	0.05±0.05	0.08±0.05	0.7±0.7	0.18±0.18	0.01±0.00	2.2±1.2	4±4	8
SR5	0.88±0.24	0.67±0.15	0.94±0.26	-	0.02±0.02	0.16±0.16	0.27±0.14	0.07±0.01	4.7±2.0	7.7±2.1	13
SR6	0.33±0.11	0.15±0.07	0.20±0.06	-	0.04±0.04	0.03±0.03	0.07±0.06	0.01±0.00	0.7±0.7	1.5±0.8	0
SR7	0.16±0.08	0.09±0.06	0.18±0.06	-	-	0.12±0.12	0.21±0.11	0.01±0.00	1.7±1.1	2.5±1.2	0
SR8	0.02±0.02	0.02±0.02	0.01±0.01	-	-	-	0.01±0.01	-	-	0.07±0.07	0

Table 12: Event yields in ML regions. Yields shown as "-" have a contribution smaller than 0.01, or do not contribute to a particular region.

	$t\bar{t}W$	$t\bar{t}Z$	$t\bar{t}H$	W Z	X+γ	Rares	Nonprompt lep.	SM expected	Data
SR1	8.7±2.2	11.1±2.8	7.0±1.9	87±23	18±11	21±11	64±24	220±40	263
SR2	0.15±0.10	0.15±0.10	0.10±0.03	1.2±0.5	0.02±0.02	0.4±0.4	0.5±0.5	2.5±2.5	1
SR3	2.3±0.6	2.0±0.5	1.6±0.4	11.9±3.2	0.24±0.12	4.2±2.2	10±4	32±6	34
SR4	0.18±0.07	0.14±0.05	0.08±0.02	0.19±0.19	-	0.20±0.20	0.11±0.11	0.9±0.5	1
SR5	1.08±0.28	1.6±0.4	1.03±0.29	10.9±3.0	0.9±0.9	1.6±0.8	4.4±1.9	22±4	28
SR6	0.91±0.23	0.64±0.16	0.58±0.16	4.8±1.3	0.05±0.02	1.1±0.6	1.5±0.6	9.5±1.8	8
SR7	27±7	29±7	22±6	6.7±1.8	7±4	11±6	110±40	210±40	265
SR8	7.9±2.0	5.0±1.2	4.6±1.2	1.2±0.4	0.8±0.4	2.4±1.2	14±5	36±6	47
SR9	3.7±1.0	5.3±1.3	3.5±0.9	1.3±0.4	0.8±0.5	1.9±1.0	5.0±2.2	21.6±3.2	20
SR10	2.7±0.7	1.7±0.4	1.8±0.5	0.50±0.17	0.28±0.13	1.0±0.5	3.6±1.6	11.6±1.9	16
SR11	22±6	19±5	16±4	0.50±0.15	6.1±3.0	5.0±2.6	15±6	84±11	105
SR12	5.0±1.3	3.0±0.7	2.9±0.8	0.08±0.02	0.63±0.32	1.3±0.7	2.6±1.0	15.5±2.1	17
SR13	3.2±0.8	4.2±1.0	3.2±0.9	0.10±0.03	0.55±0.29	1.6±0.8	2.9±1.3	15.7±2.2	21
SR14	1.5±0.4	1.27±0.30	1.21±0.34	-	0.14±0.07	0.8±0.4	0.4±0.4	5.3±0.8	8
SR15	0.90±0.24	2.0±0.5	1.9±0.6	0.02±0.01	0.25±0.13	2.5±1.3	2.6±1.4	10.2±2.1	12
SR16	4.6±1.2	4.6±1.1	3.3±0.9	5.1±1.4	1.9±1.2	3.4±1.7	4.1±1.3	27±4	40
SR17	0.14±0.07	0.18±0.07	0.05±0.02	0.24±0.24	-	0.16±0.16	-	0.8±0.5	2
SR18	3.6±0.9	2.2±0.5	2.4±0.7	3.7±1.0	0.15±0.08	3.1±1.6	2.6±1.0	17.8±2.4	24
SR19	0.25±0.09	0.16±0.06	0.07±0.02	0.17±0.12	-	0.27±0.23	0.04±0.04	1.0±0.4	0
SR20	3.3±0.9	1.7±0.4	1.6±0.5	3.7±1.1	0.10±0.05	3.1±1.6	4.3±1.9	17.8±3.0	30
SR21	0.28±0.08	0.21±0.05	0.07±0.02	0.21±0.10	-	0.37±0.21	0.11±0.11	1.26±0.33	2
SR22	1.08±0.28	46±11	1.7±0.4	610±160	11±7	100±50	48±17	830±180	955
SR23	0.71±0.18	6.8±1.7	0.45±0.12	69±18	3.1±2.7	18±9	10±4	108±22	136
SR24	0.20±0.05	8.4±2.1	0.23±0.06	93±25	0.02±0.01	12±6	2.8±1.3	117±26	139
SR25	0.16±0.05	2.0±0.5	0.17±0.05	5.8±1.6	0.03±0.01	2.2±1.1	0.8±0.6	11.1±2.3	8
SR26	0.13±0.03	7.7±1.9	0.24±0.07	85±22	2.3±1.3	11±6	3.9±1.7	111±24	128
SR27	0.09±0.02	1.4±0.4	0.06±0.02	14±4	0.7±0.7	2.4±1.3	2.0±1.1	21±5	20
SR28	0.10±0.03	2.5±0.6	0.10±0.03	34±9	-	3.7±2.0	0.7±0.4	42±10	45
SR29	0.10±0.03	0.45±0.13	0.03±0.01	2.0±0.7	-	0.61±0.31	0.22±0.14	3.4±0.9	3
SR30	5.5±1.4	140±34	6.1±1.6	52±14	5.1±2.9	70±40	40±14	320±50	408
SR31	1.7±0.4	23±6	1.15±0.31	8.3±2.3	0.19±0.10	9±5	3.6±1.8	47±8	50
SR32	0.62±0.16	26±6	0.99±0.26	11.4±3.2	0.26±0.17	9±5	2.4±1.0	51±9	62
SR33	0.31±0.08	7.5±1.8	0.35±0.10	3.5±1.1	0.04±0.02	2.8±1.5	0.6±0.5	15.1±2.6	24
SR34	4.8±1.2	88±21	4.5±1.2	3.5±1.0	2.2±1.0	22±11	5.4±2.0	131±24	157
SR35	0.97±0.26	13.3±3.2	0.76±0.21	0.72±0.20	0.09±0.04	2.7±1.4	1.5±0.9	20±4	24
SR36	0.55±0.14	20±5	0.89±0.25	0.78±0.26	0.12±0.08	3.7±1.9	0.6±0.4	27±5	36
SR37	0.24±0.06	5.2±1.2	0.34±0.09	0.39±0.13	0.05±0.03	1.2±0.6	0.4±0.4	7.8±1.5	11
SR38	0.12±0.04	9.4±2.3	0.55±0.16	0.21±0.07	0.04±0.02	2.2±1.1	0.36±0.25	12.9±2.6	18
SR39	0.52±0.14	20±5	0.85±0.24	43±11	1.8±1.0	12±6	4.3±1.3	82±14	117
SR40	0.20±0.06	3.8±0.9	0.24±0.07	8.2±2.2	0.8±0.7	3.2±1.6	1.6±0.7	18±4	26
SR41	0.35±0.10	9.3±2.2	0.47±0.14	23±6	0.01±0.01	5.3±2.7	1.2±0.5	39±8	29
SR42	0.34±0.09	1.7±0.4	0.16±0.05	1.6±0.6	0.02±0.01	0.9±0.4	0.17±0.13	4.9±0.9	7
SR43	0.30±0.08	7.0±1.7	0.19±0.05	32±9	-	6.2±3.2	0.87±0.35	46±10	44
SR44	0.34±0.09	1.7±0.4	0.12±0.03	1.9±0.6	-	1.1±0.6	0.5±0.5	5.7±1.2	11

Table 13: Event yields in LM regions. Yields shown as "-" have a contribution smaller than 0.01, or do not contribute to a particular region.

	$t\bar{t}W$	$t\bar{t}Z$	$t\bar{t}H$	W Z	WW	X+γ	Rares	Charge misid.	Nonprompt lep.	SM expected	Data
SR1	7.7±2.0	2.9±0.8	2.2±0.6	53±14	53±12	47±28	13±7	12.1±1.2	50±30	240±50	314
SR2	1.7±0.4	1.07±0.27	1.13±0.30	1.8±0.5	1.8±0.4	3.2±2.7	1.2±0.6	0.64±0.07	8±4	20±5	22
SR3	23±6	8.7±2.2	7.1±1.9	5.6±1.6	5.6±1.4	15±8	6.1±3.3	6.5±0.7	63±30	140±31	159
SR4	6.3±1.6	3.2±0.8	4.4±1.2	0.29±0.09	0.25±0.08	1.3±0.7	2.0±1.0	0.71±0.08	14±6	32±7	37
SR5	17±4	6.1±1.5	5.6±1.6	0.43±0.12	0.39±0.10	3.6±2.3	2.7±1.4	4.5±0.5	14±6	54±8	66
SR6	6.0±1.6	3.2±0.8	4.2±1.1	0.10±0.04	0.13±0.03	1.3±0.6	2.0±1.0	0.65±0.07	4.3±2.7	22±4	33
SR7	2.4±0.6	1.21±0.30	1.4±0.4	0.07±0.03	-	0.6±0.4	2.1±1.1	0.51±0.05	1.4±1.4	9.7±2.1	23
SR8	0.10±0.05	0.01±0.01	0.02±0.01	0.22±0.10	0.80±0.20	-	0.04±0.02	0.06±0.01	0.28±0.28	1.5±0.5	3
SR9	0.36±0.10	0.15±0.05	0.11±0.03	0.16±0.05	0.11±0.03	0.18±0.11	0.19±0.10	0.03±0.00	0.28±0.28	1.6±0.4	1
SR10	0.16±0.08	0.04±0.03	0.01±0.01	0.23±0.14	0.78±0.24	1.3±1.3	0.09±0.09	0.06±0.02	0.16±0.16	2.9±2.9	1
SR11	0.46±0.15	0.01±0.01	0.08±0.03	-	0.13±0.07	0.02±0.02	0.15±0.11	0.04±0.02	1.0±1.0	1.9±1.4	3